



Topology optimization of steady Navier–Stokes flow with body force



Yongbo Deng, Zhenyu Liu*, Junfeng Wu, Yihui Wu*

State Key Laboratory of Applied Optics, Changchun Institute of Optics, Fine Mechanics and Physics (CIOMP), Chinese Academy of Sciences, 130033 Changchun, Jilin, China

ARTICLE INFO

Article history:

Received 7 May 2012

Received in revised form 14 November 2012

Accepted 18 November 2012

Available online 5 December 2012

Keywords:

Topology optimization

Body force

Level set method

Topological sensitivity

Continuous adjoint method

ABSTRACT

This paper presents the topology optimization of steady Navier–Stokes flows with body forces that influence the optimal shape and topology of fluid flows. Based on the implicit expression of the fluid flow with the level set method, an optimization problem is formulated and analyzed using the continuous adjoint method. The shape and topological sensitivities are computed based on the adjoint and asymptotic analysis of the optimization problem. In the optimization procedure, the level set surface is evolved based on the shape sensitivity and nucleated based on the topological sensitivity simultaneously. Three kinds of body forces that are commonly used in the design of fluid devices, i.e. constant, nonuniform, and solution-dependent body forces, are considered in the two-dimensional and three-dimensional numerical examples. Numerical results demonstrate that this method can effectively achieve the topology optimization of the Navier–Stokes flows with body forces.

© 2012 Elsevier B.V. All rights reserved.

1. Introduction

Topology optimization method has gained much attention for the design of mechanisms and functional materials [1]. The goal of topology optimization is not only to modify the shape of the structural boundaries but also to allow for a change in the connectiveness of the structural domain. Several approaches, such as the evolutionary techniques [2], the homogenization method [3,4], the density method [5,6] and the level set method [7–10], have been developed for the implementation of topology optimization. Topology optimization for fluid problems was pioneered by Steven et al. using the evolutionary techniques [2]. On the density method, Borrvall and Petersson performed the first attempt for the Stokes flow [11]. An artificial friction force that is proportional to the fluid velocity was added to the Stokes equations in order to smoothly interpolate between the solid and fluid regions. Recently, this optimization model was extended to the Navier–Stokes flows with low and moderate Reynolds numbers [12–16]. In the Navier–Stokes flows, external body forces that relate with the fluid inertia effect, such as the gravity, centrifugal force and Coriolis force, usually exist. Therefore, it is necessary to develop a topology optimization method for the Navier–Stokes flows with body forces. However, the optimization model proposed by Borrvall and Petersson in [11] is hard to be extended directly to the flows with external forces. One of the reasons is that the two kinds of force terms exist in the Navier–Stokes equations, i.e. external force which has

specific physical meaning, and the artificial friction force which is used to control the topology of fluid domains. Typically, the interpolation of artificial friction force must be modified so that the external body force can drive the motion of fluid and the artificial friction force can modify the topology of the fluid domain reasonably. A similar problem exists for the topology optimization of mechanisms using the density method. The standard interpolation function, such as the solid isotropic material with penalization (SIMP), has been used successfully for designing mechanisms with fixed loads. However, the SIMP can not be used directly to design mechanisms when the body forces (also called design-dependent loads), such as the self-weight of a structure or centrifugal force, are used as loads [17–19]. To overcome the above challenge, one can either modify the interpolation function for the design variable [20], or implement topology optimization using the level set method [8]. For both of these strategies, the key point is to choose a suitable way to deal with the design-dependent loads. In this paper, the variational level set method is used to extend the topology optimization method to the Navier–Stokes flows with body forces. Naturally, this method is suitable for the flows without body forces. The level set method pioneered by Osher and Sethian [21], Osher and Fedkiw [22] and Sethian [23] accomplishes the change of topology by evolving and merging the level set surface. This method provides a general way to track the implicit interface between two phases, and it has been applied to image processing [24], interface tracking of two-phase flow [25], and shape optimization [26,27]. In optimization, the major advantage of the level set method lies in expressing continuously moving interfaces and abstracting the material domains that correspond to the structural topology. In some applications, it has been observed that the

* Corresponding author.

E-mail addresses: dengyb@ciomp.ac.cn (Y. Deng), liuzy@ciomp.ac.cn (Z. Liu), yihuiwu@ciomp.ac.cn (Y. Wu).

conventional level set method may be inadequate for the cases in which the initial shape of the structure has fewer holes than the optimal geometry [8], especially in the two-dimensional cases. The above difficulty can be overcome using topological sensitivity, which was introduced by Sokolowski and Zochowski [28] for linear elasticity and has been extended to several other linear and nonlinear physical problems [29–32]. In particular, the topological sensitivity has been researched for the Stokes flows [33–36] and Navier–Stokes flows [37].

This paper considers the topology optimization method for the Navier–Stokes flows with body forces, where the optimization is implemented by the variational level set method considering the shape and topological sensitivities simultaneously. The solid and fluid domains are distinguished by constraining the fluid velocity to vanish in solid domain. Based on the continuous adjoint method, the shape and topological sensitivities for two commonly used objectives, the dissipation power and the reverse of the kinetic energy, are considered separately. Flows driven by body forces have been widespread used in the fluid devices. Therefore, this topology optimization method can be used to perform the optimal design of the fluid devices with constant, nonuniform and solution-dependent forces.

The remainder of this paper is organized as follows: in Section 2, the approach of coupling the Navier–Stokes equations with the level set method is introduced, an optimization problem is formulated and analyzed using the Lagrange multiplier based adjoint method; in Section 3, the shape and topological sensitivities are derived for different optimization objectives; in Section 4, several details on the numerical implementation of the topology optimization method are discussed; in Section 5, several numerical examples are presented for the Navier–Stokes flows with constant (gravity), nonuniform (centrifugal force) and solution-dependent body forces (Coriolis force) to demonstrate the feasibility and necessity of the topology optimization method for the Navier–Stokes flows with body forces.

2. Topology optimization problem

2.1. Navier–Stokes flow with implicit boundary expressed using level set method

In order to express the solid–liquid boundary implicitly, the incompressible Navier–Stokes equations can be coupled with the level set function that is expressed by a signed distance function ϕ defined on an optimization domain $\Omega \subset \mathbb{R}^d \rightarrow \mathbb{R}$ ($d = 2$ or 3 is the spatial dimension, and Ω is open). The solid and fluid regions can be distinguished as follows:

$$\begin{cases} \phi(\mathbf{x}) > 0, & \forall \mathbf{x} \in \Omega_s \\ \phi(\mathbf{x}) < 0, & \forall \mathbf{x} \in \Omega_f \\ \phi(\mathbf{x}) = 0, & \forall \mathbf{x} \in \Gamma \end{cases} \quad (1)$$

where Ω_s , Ω_f and Γ are the solid region, fluid region and implicit boundary respectively; Ω_s and Ω_f are open, and they satisfy $\bar{\Omega}_s \cup \bar{\Omega}_f = \bar{\Omega}$ (Fig. 1). Then the incompressible Navier–Stokes equations can be modified by constraining the fluid velocity to be zero in the solid region Ω_s :

$$\begin{cases} -\eta \Delta \mathbf{u} + \rho(\mathbf{u} \cdot \nabla) \mathbf{u} + \nabla p = \mathbf{f} & \text{in } \Omega \\ -\nabla \cdot \mathbf{u} = 0 & \text{in } \Omega \\ H(\phi) \mathbf{u} = \mathbf{0} & \text{in } \Omega \end{cases} \quad (2)$$

where η is the dynamic viscosity; ρ is the density of the fluid; \mathbf{u} is the fluid velocity; p is the fluid pressure; and \mathbf{f} is the body force. Particularly, if a domain $\Omega_c \subset \Omega$ (Ω_c is open) needs to be a solid

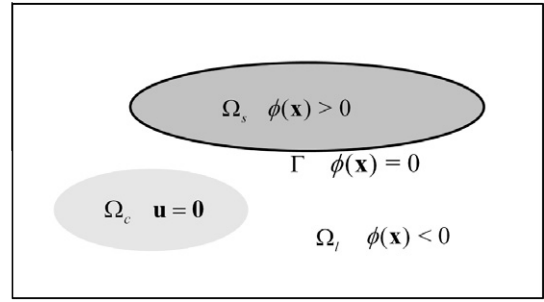


Fig. 1. Schematic of the regions distinguished based on the level set function.

region throughout an optimization procedure, one can constrain the fluid velocity to be zero in Ω_c (Fig. 1)

$$\mathbf{u} = \mathbf{0} \quad \text{in } \Omega_c \quad (3)$$

In the above, $H(\phi)$ is the Heaviside function [21]:

$$H(\phi) = \begin{cases} 1, & \phi \geq 0 \\ 0, & \phi < 0 \end{cases} \quad (4)$$

and the derivative of $H(\phi)$ to ϕ is the Dirac function $\tau(\phi)$. In most cases, the Heaviside function and the Dirac function need to be regularized from the numerical implementation point of view. In this paper, $H(\phi)$ and $\tau(\phi)$ are approximated by the smoothed Heaviside function and Dirac function [49]:

$$H(\phi) = \begin{cases} 0, & \phi \leq -h \\ \frac{1}{2} + \frac{15\phi}{16h} - \frac{5\phi^2}{8h^2} + \frac{3\phi^3}{16h^3}, & -h < \phi < h \\ 1, & \phi > h \end{cases} \quad (5)$$

$$\tau(\phi) = \begin{cases} \frac{15}{16h} \left(1 - \frac{\phi^2}{h^2}\right)^2, & |\phi| \leq h \\ 0, & |\phi| > h \end{cases} \quad (6)$$

where h is the support size (Fig. 2). For more details on the regularization of the Heaviside function, one can refer to [38–40]. In this paper, the support size h of the smoothed Heaviside function and the Dirac function is kept as constant during the optimization procedure [7,8,27,31].

Usually, fluid flows have a known velocity or pressure distribution at the inlet boundary. For the velocity boundary case, the given velocity distribution \mathbf{u}_{in} imposed on the inlet Γ_{in} of the computational domain Ω is

$$\mathbf{u} = \mathbf{u}_{in} \quad \text{on } \Gamma_{in} \quad (7)$$

where Γ_{in} belongs to the Dirichlet boundary Γ_D . For the pressure boundary case, the given pressure distribution p_0 with the zero viscous stress of flow is imposed on the inlet Γ_{in} of the computational domain Ω :

$$\begin{cases} p = p_0 & \text{on } \Gamma_{in} \\ \eta(\nabla \mathbf{u} + \nabla \mathbf{u}^T) \cdot \mathbf{n} = \mathbf{0} & \text{on } \Gamma_{in} \end{cases} \quad (8)$$

In this case, the pressure condition on Γ_{in} belongs to the Dirichlet boundary condition, and the zero viscous stress condition on Γ_{in} belongs to the Neumann boundary condition. For both the velocity and pressure inlet boundary cases, the outlet boundary condition is usually set to be:

$$[-p\mathbf{I} + \eta(\nabla \mathbf{u} + \nabla \mathbf{u}^T)] \cdot \mathbf{n} = \mathbf{g} \quad \text{on } \Gamma_{out} \quad (9)$$

where $\mathbf{g} = \mathbf{0}$ corresponds to the open boundary condition and Γ_{out} belongs to the Neumann boundary Γ_N . For the case that the flow is driven by the body force, the open boundary condition expressed by Eq. (9) can be imposed on both the inlet and outlet. The other

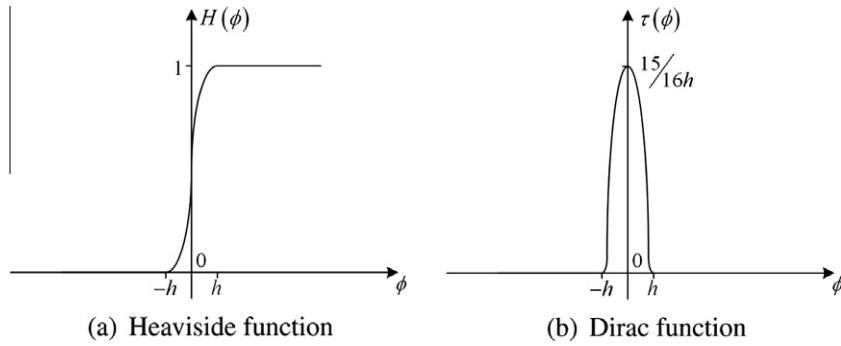


Fig. 2. Smoothed Heaviside function and Dirac function.

boundaries of the computational domain Ω are no-slip type where $\mathbf{u} = \mathbf{0}$.

For an optimization problem, the objective is chosen according to the description of the desired result and characteristics of the forward physical problems. For the flow with a fixed velocity distribution at the inlet, minimizing the dissipated power is equivalent to minimizing the pressure drop across the fluid system. Therefore, the characteristic of the flow can be measured by the dissipation power [11,13,27]:

$$J_d(\nabla \mathbf{u}; \phi) = \int_{\Omega} \frac{1}{2} \eta H(-\phi) (\nabla \mathbf{u} + \nabla \mathbf{u}^T) : (\nabla \mathbf{u} + \nabla \mathbf{u}^T) d\Omega \quad (10)$$

For the flow with a fixed pressure distribution at the inlet, the optimization of the flow can be performed by maximizing the kinetic energy stored in the fluid system. Then the reverse of the kinetic energy can be chosen to be the objective:

$$J_k(\mathbf{u}; \phi) = - \int_{\Omega} \frac{1}{2} \rho H(-\phi) \mathbf{u}^2 d\Omega \quad (11)$$

For the body force driven flow, both the expression in Eqs. (10) and (11) can be used as the objective of the optimization problem.

2.2. Topology optimization problem for Navier–Stokes flow with body force

Based on the description in Section 2.1, the topology optimization problem for the Navier–Stokes flows with body forces can be expressed as:

$$\text{Min} : J(\mathbf{u}, \nabla \mathbf{u}, p; \phi) = \int_{\Omega} H(-\phi) A(\mathbf{u}, \nabla \mathbf{u}, p) d\Omega + \int_{\Gamma} B(\mathbf{u}, p) d\Gamma$$

$$\begin{aligned} \text{S.t.} \quad & \int_{\Omega} H(-\phi) d\Omega = V^* V_{\Omega} \\ & -\eta \Delta \mathbf{u} + \rho(\mathbf{u} \cdot \nabla) \mathbf{u} + \nabla p = \mathbf{f} \text{ in } \Omega \\ & -\nabla \cdot \mathbf{u} = 0 \text{ in } \Omega \\ & H(\phi) \mathbf{u} = \mathbf{0} \text{ in } \Omega \\ & \mathbf{u} = \mathbf{0} \text{ in } \Omega_c \end{aligned} \quad (12)$$

where $A(\mathbf{u}, \nabla \mathbf{u}, p)$ and $B(\mathbf{u}, p)$ are the functionals defined on the domain Ω and implicit boundary Γ , respectively; $V^* \in (0, 1)$ is the volume fraction of the fluid region; and V_{Ω} is the volume of the optimization domain Ω . The objective of the optimization problem in Eq. (12) can be transformed into the following formulation:

$$J(\mathbf{u}, \nabla \mathbf{u}, p; \phi) = \int_{\Omega} [H(-\phi) A(\mathbf{u}, \nabla \mathbf{u}, p) + \tau(\phi) \|\nabla \phi\| B(\mathbf{u}, p)] d\Omega \quad (13)$$

For the optimization problem in Eq. (12), the evolution of the level set function is performed by solving the Hamilton–Jacobi equation [31,41]:

$$\frac{\partial \phi}{\partial t} + V_n \|\nabla \phi\| + \omega G = 0 \quad (14)$$

where V_n is the normal evolving velocity of the level set function ϕ ; G is the topological sensitivity; and ω is the weight of the topological sensitivity. In this paper, the reasonable weight of topological sensitivity is chosen based on numerical experiments. Based on the empirical insight, the new zero level set can not be nucleated if the weight of topological sensitivity is too low; numerical instability is produced if the weight of topological sensitivity is too high; and relative large weight should be chosen as the Reynolds number of the flow is increased. Based on the work of Osher and Sethian [21], the level set function is evolved along the steepest direction using the transformed formulation of Eq. (14):

$$\delta \phi + V_n \|\nabla \phi\| \delta t + \omega G \delta t = 0 \quad (15)$$

where δt is the positive evolution time. As pointed out by Jung et al. in [42], Eq. (15) is equivalent to Hamilton–Jacobi equation (14) if the change of the distance function is viewed as occurring continuously in time.

3. Sensitivity analysis

3.1. Shape sensitivity analysis

The algorithm used to update the level set function in this paper belongs to the gradient descent method. The normal velocity is a measure of the continuum gradient of objective to the level set function. In the following, the Lagrangian multiplier based adjoint method [43–46] are used to perform the sensitivity analysis of the topology optimization problem in Eq. (12). According to the Lagrangian multiplier method, the Lagrangian corresponding to the objective in Eq. (12) is introduced as

$$\begin{aligned} \hat{J} = & J(\mathbf{u}, \nabla \mathbf{u}, p; \phi) + a(\mathbf{u}, \mathbf{w})_{\Omega} + b(\mathbf{u}; \mathbf{u}, \mathbf{w})_{\Omega} - (p, \nabla \cdot \mathbf{w})_{\Omega} \\ & - (\mathbf{f}, \mathbf{w})_{\Omega} - (\nabla \cdot \mathbf{u}, q)_{\Omega} + (H(\phi) \mathbf{u}, \mathbf{w})_{\Omega} + (\mathbf{u}, \mathbf{w})_{\Omega_c} \\ & - \lambda \left(\int_{\Omega} H(-\phi) d\Omega - V^* V_{\Omega} \right) + \frac{\Lambda}{2} \left(\int_{\Omega} H(-\phi) d\Omega - V^* V_{\Omega} \right)^2 \\ & - \int_{\Gamma_D} \mathbf{g} \cdot \mathbf{w} d\Gamma + \int_{\Gamma_D} \mathbf{u} \cdot \mathbf{w} d\Gamma \end{aligned} \quad (16)$$

where $a(\mathbf{u}, \mathbf{w})_{\Omega} = \eta \int_{\Omega} \nabla \mathbf{u} : \nabla \mathbf{w} d\Omega$; $b(\mathbf{u}; \mathbf{u}, \mathbf{w})_{\Omega} = \rho \int_{\Omega} (\mathbf{u} \cdot \nabla) \mathbf{u} \cdot \mathbf{w} d\Omega$; $(\cdot, \cdot)_{\Omega}$ is the Hilbert inner product; \mathbf{w} and q are the adjoint variables of the fluid velocity \mathbf{u} and the pressure p , respectively. The velocity $\mathbf{u} \in \mathcal{H}_E^1(\Omega) := \{\mathbf{u} \in \mathcal{H}^1(\Omega) \mid \mathbf{u} = \mathbf{u}_D \text{ on } \Gamma_D\}$, where \mathbf{u}_D is the known velocity distribution on Γ_D ; the adjoint variable $\mathbf{w} \in \mathcal{H}_{E_0}^1(\Omega) := \{\mathbf{w} \in \mathcal{H}^1(\Omega) \mid \mathbf{w} = \mathbf{0} \text{ on } \Gamma_D\}$, and $p, q \in \mathcal{L}^2(\Omega)$. Therefore, $(\mathbf{u}, \mathbf{w})_{\Omega_c}$ and $\int_{\Gamma_D} \mathbf{u} \cdot \mathbf{w} d\Gamma$ are equal to zero. The volume constraint is treated by the augmented Lagrangian method, where $\lambda \in \mathbb{R}$ is the Lagrangian multiplier and $\Lambda \in \mathbb{R}$ is the penalty parameter. According to the Lagrangian multiplier based adjoint method, the adjoint equations

of the Navier–Stokes equations with body force can be expressed as (see Appendix A.1 for more details):

$$\begin{aligned}
 & -\eta \Delta \mathbf{w} + \rho \mathbf{w} \cdot (\nabla \mathbf{u}) - \rho (\mathbf{u} \cdot \nabla) \mathbf{w} + \nabla q = -\frac{\partial \tilde{A}}{\partial \mathbf{u}} + \nabla \cdot \frac{\partial \tilde{A}}{\partial \nabla \mathbf{u}} + \frac{\partial \mathbf{f}}{\partial \mathbf{u}} \cdot \mathbf{w} \quad \text{in } \Omega \\
 & -\nabla \cdot \mathbf{w} = -\frac{\partial \tilde{A}}{\partial p} + \frac{\partial \mathbf{f}}{\partial p} \cdot \mathbf{w} \quad \text{in } \Omega \\
 & \mathbf{w} = \mathbf{0} \quad \text{on } \Gamma_D \\
 & [-q \mathbf{I} + \eta (\nabla \mathbf{w} + \nabla \mathbf{w}^T)] \cdot \mathbf{n} = -\rho (\mathbf{u} \cdot \mathbf{n}) \mathbf{w} - \frac{\partial \tilde{A}}{\partial \nabla \mathbf{u}} \cdot \mathbf{n} \quad \text{on } \Gamma_N
 \end{aligned} \tag{17}$$

where $\tilde{A} = H(-\phi)A + \tau(\phi)\|\nabla\phi\|B$. Compared with the adjoint analysis of the Navier–Stokes equations without body force [47,48], Eq. (17) contains the derivatives of the body force to the unknown variables \mathbf{u} and p . The shape sensitivity for the optimization problem in Eq. (12) is obtained as (see Appendix A.2 for more details):

$$\begin{aligned}
 \delta \hat{J} = & -\int_{\Omega} \left[A + \nabla B \cdot \mathbf{n}_{\Gamma} + B\kappa - \mathbf{u} \cdot \mathbf{w} - \lambda \right. \\
 & \left. + \Lambda \left(\int_{\Omega} H(-\phi) d\Omega - V^* V_{\Omega} \right) \right] \tau(\phi) \delta \phi d\Omega
 \end{aligned} \tag{18}$$

where $\mathbf{n}_{\Gamma} = \nabla \phi / \|\nabla \phi\|$ and $\kappa = \nabla \cdot \mathbf{n}_{\Gamma}$. To ensure the descendant of the objective, the shape sensitivity should satisfy $\delta \hat{J} < 0$. According to Eq. (15), the variational of the level set function is $\delta \phi = -V_n \|\nabla \phi\| \delta t$ in the shape sensitivity analysis. Because $\tau(\phi)$, $\|\nabla \phi\|$ and δt are all nonnegative, the normal velocity for evolving the level set function can be set to be

$$V_n = -A - \nabla B \cdot \mathbf{n}_{\Gamma} - B\kappa + \mathbf{u} \cdot \mathbf{w} + \lambda - \Lambda \left(\int_{\Omega} H(-\phi) d\Omega - V^* V_{\Omega} \right) \tag{19}$$

3.2. Topological sensitivity analysis

Topological sensitivity measures the change of a cost function with respect to a topological modification of a domain. The most simple way of modifying the topology consists in creating a small hole in the domain. In structural optimization, creating a hole means removing some material. However, in fluid optimization, where the domain represents the fluid, creating a hole means inserting an obstacle [35]. In the level set method, topological sensitivity measures the change of the objective value by incorporating small holes corresponding to the new level set to change the topology of the fluid domain. Such perturbation is continuous in the \mathcal{L}^1 -distance of sets [31]. Topological sensitivity is defined as:

$$d_{\mathcal{T}} \hat{J}(\Omega)(\mathbf{x}) = \lim_{r \rightarrow 0} \frac{\hat{J}(\Omega_{r,\mathbf{x}}) - \hat{J}(\Omega)}{\|B_{r,\mathbf{x}} \cap \Omega\|_{\mathcal{L}}}, \quad \forall \mathbf{x} \in \bar{\Omega} \tag{20}$$

where $B_{r,\mathbf{x}} = \{\mathbf{y} \mid \|\mathbf{y} - \mathbf{x}\|_{\mathcal{L}} < r\}$, $\Omega_{r,\mathbf{x}} = \Omega \setminus \overline{B_{r,\mathbf{x}}}$ and $\|\cdot\|_{\mathcal{L}}$ denotes the Lebesgue measure of a set. Based on the asymptotic analysis of Eq. (20) for the Navier–Stokes equations [37], the topological sensitivity can be expressed as:

$$d_{\mathcal{T}} \hat{J}(\Omega)(\mathbf{x}) = \begin{cases} 4\pi\rho\eta\mathbf{u} \cdot \mathbf{w} + d_{\mathcal{T}}J(\Omega)(\mathbf{x}) - (\lambda - \Lambda V)d_{\mathcal{T}}V(\Omega)(\mathbf{x}), & \text{in 2D} \\ 6\pi\rho\eta\mathbf{u} \cdot \mathbf{w} + d_{\mathcal{T}}J(\Omega)(\mathbf{x}) - (\lambda - \Lambda V)d_{\mathcal{T}}V(\Omega)(\mathbf{x}), & \text{in 3D} \end{cases} \tag{21}$$

where \mathbf{w} is the adjoint variable of \mathbf{u} , $V = \int_{\Omega} H(-\phi) d\Omega - V^* V_{\Omega}$ is the residual of the volume constraint. In Eq. (21), $d_{\mathcal{T}}J(\Omega)(\mathbf{x})$ depends on the embody of the objective J . For the topology optimization problem in Eq. (12), $d_{\mathcal{T}}J(\Omega)(\mathbf{x})$ can be determined by the asymptotic expansion of J :

$$J(\Omega_{r,\mathbf{x}}) - J(\Omega) = f(r)d_{\mathcal{T}}J(\Omega)(\mathbf{x}) + o(f(r)) \tag{22}$$

where $f(r)$ is a positive function satisfying $\lim_{r \rightarrow 0} f(r) = 0$. According to [37], $f(r)$ should be chosen as $-1/\ln r$ in two dimensional case or r in three dimensional case. Therefore, the topological sensitivity for the objectives in Eqs. (10) and (11) can be expressed as:

$$d_{\mathcal{T}}J_d(\Omega)(\mathbf{x}) = \begin{cases} 4\pi\rho\eta\mathbf{u} \cdot \mathbf{u}, & \text{in 2D} \\ 6\pi\rho\eta\mathbf{u} \cdot \mathbf{u}, & \text{in 3D} \end{cases} \tag{23}$$

and

$$d_{\mathcal{T}}J_k(\Omega)(\mathbf{x}) = 0 \tag{24}$$

respectively. The topological sensitivity related with the residual of volume constraint can be expressed as:

$$d_{\mathcal{T}}V(\Omega)(\mathbf{x}) = \begin{cases} -\pi, & \text{in 2D} \\ -\frac{4}{3}\pi, & \text{in 3D} \end{cases} \tag{25}$$

Therefore, the topological sensitivity for the optimization problem in Eq. (16) are

$$d_{\mathcal{T}}\hat{J}_d(\Omega)(\mathbf{x}) = \begin{cases} 4\pi\rho\eta\mathbf{u} \cdot (\mathbf{w} + \mathbf{u}) + \pi[\lambda - \Lambda(\int_{\Omega} H(-\phi) d\Omega - V^*V_{\Omega})], & \text{in 2D} \\ 6\pi\rho\eta\mathbf{u} \cdot (\mathbf{w} + \mathbf{u}) + \frac{4\pi}{3}[\lambda - \Lambda(\int_{\Omega} H(-\phi) d\Omega - V^*V_{\Omega})], & \text{in 3D} \end{cases} \tag{26}$$

when the objective is the dissipation power in Eq. (10); and

$$d_{\mathcal{T}}\hat{J}_k(\Omega)(\mathbf{x}) = \begin{cases} 4\pi\rho\eta\mathbf{u} \cdot \mathbf{w} + \pi[\lambda - \Lambda(\int_{\Omega} H(-\phi) d\Omega - V^*V_{\Omega})], & \text{in 2D} \\ 6\pi\rho\eta\mathbf{u} \cdot \mathbf{w} + \frac{4\pi}{3}[\lambda - \Lambda(\int_{\Omega} H(-\phi) d\Omega - V^*V_{\Omega})], & \text{in 3D} \end{cases} \tag{27}$$

when the objective is the reverse of the kinetic energy in Eq. (11). The topology of the fluid domain can be modified by nucleating the level set surface. Numerically, the above procedure can be implemented by solving Eq. (14) and setting G to be $d_{\mathcal{T}}\hat{J}(\Omega)(\mathbf{x})$. For more details on the asymptotic analysis of the Navier–Stokes equations for the topological sensitivity, one can refer to Amstutz's work in [32,37].

4. Numerical implementation

The flowchart of the optimization procedure includes the following steps (Fig. 3): (a) the initial distribution of the level set function ϕ , the initial values of the Lagrangian multiplier λ_0 and the penalty parameter Λ_0 are given; (b) the velocity \mathbf{u} and the pressure p are computed by solving the Navier–Stokes equation (2), and the corresponding adjoint variables \mathbf{w} and q are computed by solving the adjoint equation (17); (c) the normal velocity V_n and the topological sensitivity G are computed; (d) the level set function ϕ is evolved by solving the Hamilton–Jacobi equation (14); (e) the level set function ϕ is reinitialized after several iterations; (f) the iterative optimization is stopped when the change of the objective values and the volume constraint are less than the user-specified tolerance 1×10^{-3} in five consecutive iterations. The level set function is evolved on a grid mesh with ghost elements (the composition of the dash and solid mesh in Fig. 4). The mesh for solving the Navier–Stokes equations is a set of elements embedded in the grid mesh for evolving the level set function (solid mesh in Fig. 4). The Navier–Stokes equations and the adjoint equations are solved by the commercial software *COMSOL Multiphysics* [49]. One of the advantages of the *COMSOL Multiphysics* software is that one can input the user-defined partial differential equations (PDEs) using the so-called *general PDE* form in the software's graphic user interface. Therefore, both the Navier–Stokes equations and the corresponding adjoint equations are defined in *COMSOL* and solved using the standard Galerkin finite element discretization. During the optimization procedure, the Navier–Stokes equations and the adjoint equations are solved by the Taylor–Hood Q2-Q1 elements [50], which interpolate the fluid velocity quadrat-

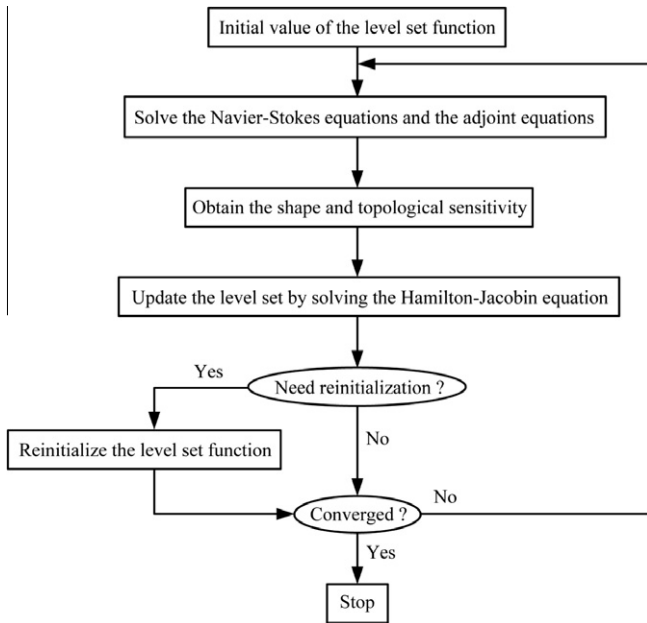


Fig. 3. Flowchart of the optimization procedure for solving the optimization problem in Eq. (12).

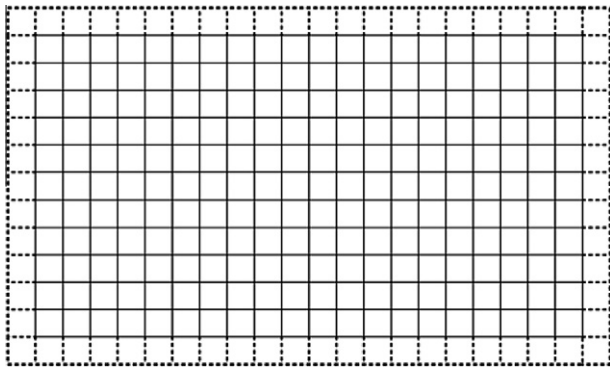


Fig. 4. Meshes used for solving the Navier–Stokes equations (solid mesh) and evolving the level set function (composition of the solid and dash meshes).

ically and the fluid pressure linearly. The level set function is interpolated by the linear Q1 elements. The Lagrangian multiplier λ and the penalty parameter Λ are updated as [44,45]:

$$\begin{aligned} \lambda_k &= \lambda_{k-1} - \Lambda_{k-1} \left(\int_{\Omega} H(-\phi_{k-1}) d\Omega - V^* V_{\Omega} \right) \\ \Lambda_k &= \frac{1}{\alpha} \Lambda_{k-1}, \quad \alpha \in (0, 1) \end{aligned} \quad (28)$$

To evolve the level set function, the Hamilton–Jacobi equation is solved by the upwind finite difference method. The time step for the finite difference scheme is chosen based on the CFL stability condition [51]:

$$\Delta t \leq \beta \frac{h_E}{\max\{|V_n|\}}, \quad \beta \in (0, 1) \quad (29)$$

where h_E is the size of the elements and β is chosen as 0.1 in this paper. The evolved level set function is reinitialized after several iterations. The reinitialization of the level set function can be performed by solving the Eikonal equation [52]:

$$\begin{cases} \|\nabla\phi\| = 1 \\ \text{sgn}(\phi) = \text{sgn}(\phi_0) \end{cases} \quad (30)$$

where sgn denotes the sign value, which is either 1, -1 or 0; ϕ_0 is the unreinitialized level set function. Eq. (30) is solved by computing the Euclidean distance transform of the binary value that corresponds to the level set function [41].

5. Numerical examples

In this section, the topology optimization of the Navier–Stokes flow by the variational level set method considering the shape and topological sensitivities is validated firstly. Then the optimization is implemented for the Navier–Stokes flows with constant, nonuniform and solution-dependent body forces respectively. The density ρ and the viscosity η are set to be unit in the following numerical examples. The signed distance function is reinitialized after every five iterations. The Heaviside function and the Dirac function are approximated with the support size $h = 1.5h_E$, where h_E is the size of the elements [51]. Based on numerical experiments, the initial values of α , the Lagrangian multiplier λ and the penalty parameter Λ in Eq. (28) are chosen as 9×10^{-1} , -1×10^{-2} and 1×10^{-3} , respectively.

5.1. Validation of topology optimization by considering shape and topological sensitivities for Navier–Stokes flow

To validate the topology optimization of the Navier–Stokes flow using the variational level set method considering the shape and topological sensitivities, a four-terminal device is optimized. The obtained results are compared with those obtained by Olesen et al. using the density method [13]. For the convenience of comparison, all of the data are chosen the same as those in [13], including the optimization domain (Fig. 5(a)), the boundary conditions (parabolic velocity distribution at the inlets, zero pressure and normal flow at the outlets), the objective function (Eq. (10)), and the volume fraction ($V^* = 0.4$) for the volume constraint. The optimization domain is discretized by 70×100 rectangular elements. The Reynolds number is defined as $\text{Re} = \rho U_{\max} L / \eta$, where U_{\max} is the maximal value of the parabolic velocity distribution imposed on the inlet and L is the width of the inlet. The initial level set function and the corresponding zero contours are shown in Fig. 5(b) and (c). By solving the optimization problem in Eq. (12) for the flows with Reynolds numbers 20 and 200 respectively, the optimized results are obtained as shown in Fig. 6. By observing the evolving procedure of the level set, it is clear that the topological sensitivity can nucleate new level set effectively (Figs. 7 and 10). Snapshots for the unitary shape sensitivity and topological sensitivity distributions are shown in Figs. 8, 9, 11 and 12, respectively. As the Reynolds number is increased, the dissipation of the fluid stream caused by the bending channel grows. When the inertia effect dominates the flow with a large Reynolds number, larger velocity gradients appear in the bend channels. This increases the dissipation compared to the low Reynolds number case. Therefore, the optimized four-terminal device has two bending channels for the flow with low Reynolds number, and has two paralleling straight channels for the larger Reynolds number case. This is consistent with the conclusion obtained by Gersborg-Hansen et al. in [12].

5.2. Constant body force

5.2.1. Horizontal channel in gravity

A constant body force, e.g. the gravity, is the simplest body force in the Navier–Stokes equations. For the constant body force case, the horizontal flows with velocity and pressure boundary conditions imposed on the inlet are optimized respectively. The optimization domain are shown in Fig. 13(a), where the domain is

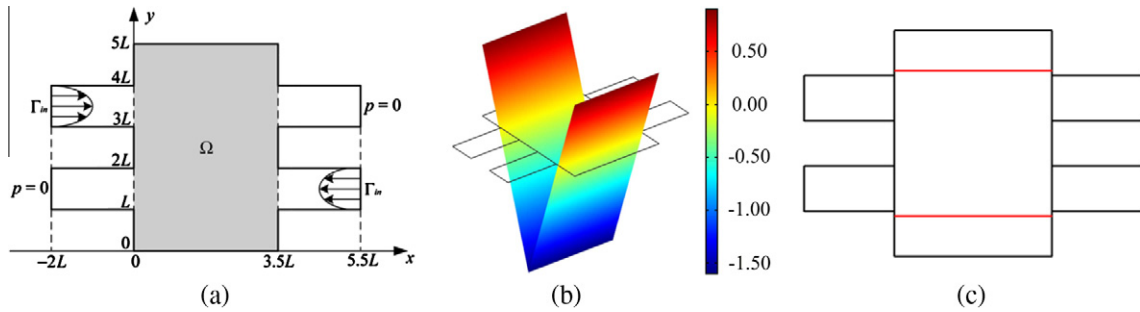


Fig. 5. (a) Optimization domain (gray region) and computational domain (gray region and four ducts) of the four-terminal device; (b) initial distribution of the level set function; (c) zero level set of the initial level set function.

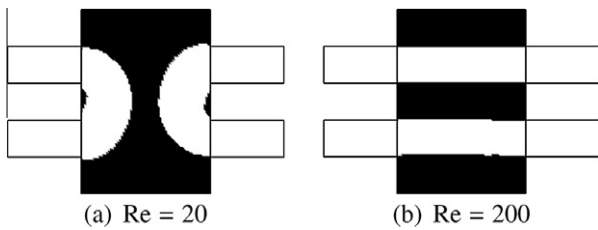


Fig. 6. Optimized topology of the four-terminal device with Reynolds numbers equal to 20 and 200, respectively.

discretized by 360×120 rectangular elements. The initial level set function is set to be the solution of Eq. (30), where the initial value ϕ_0 is specified as -1 (Fig. 13(b)). Because the value of ϕ_0 is less than zero, the initial level set function has no zero level set. The zero level set will be nucleated with the help of the topological sensitivity. The volume fraction of the fluid region V^* is set to be 0.4. The constant body force \mathbf{f} is set to be the gravity $\mathbf{g} = (0, -10)$. The optimized channel is shown in Fig. 14(a) for the flow with a specified parabolic velocity distribution at the inlet, where the maximal value of the specified velocity is 1 and the objective is chosen to be the dissipation power (Eq. (10)). The convergent history of the objective value and the volume constraint is shown in Fig. 15. By comparing with the optimized channel for the case without the gravity (Fig. 14(b)), the gravity causes the bending of the horizontal channel. For the case of inlet boundary with a given pressure distribution (Eq. (8)), where the value of pressure is chosen to be 30, so that the flux at the inlet is the same as the velocity

boundary case. The optimized channel is shown in Fig. 16 by using the reverse of the kinetic energy (Eq. (11)) as objective. In the above numerical examples, the weight of the topological sensitivity ω is set to be 2. The results in Figs. 14(a) and 16 show that the optimized channels bend to the direction of the gravity, where extra work is imposed on the fluid. For the flow with velocity boundary condition, the work decreases the pressure drop between the inlet and outlet. This is equivalent to decrease the value of the dissipated power inside the optimized channel. For the flow with pressure boundary condition, the work done by the gravity is translated into the kinetic energy of the fluid partly, which helps to increase the kinetic energy of the flow. Therefore, similar topologies are obtained for both the cases of inlet boundary with known velocity and pressure distribution.

5.2.2. Four-terminal device in gravity

This numerical example performs the optimization of a four-terminal device in the gravity. The four-terminal device has two inlets with given parabolic velocity distributions, and the other two terminals are outlets with open boundary condition (Fig. 17(a)). The maximal value of the velocity imposed on the inlets is 1. The optimization domain is discretized by 60×60 rectangular elements. The initial level set function is set to be the solution of Eq. (30), where the initial value ϕ_0 is specified as -1 (Fig. 17(b)). Because the value of ϕ_0 is less than zero, the initial level set function has no zero level set. The zero level set will be nucleated with the help of the topological sensitivity. The weight of the topological sensitivity ω and the volume fraction of fluid V^* are set to be 2 and 0.4, respectively. After solving the optimization problem in Eq. (12) with dissipation power (Eq. (10)) as objective, the optimized topol-

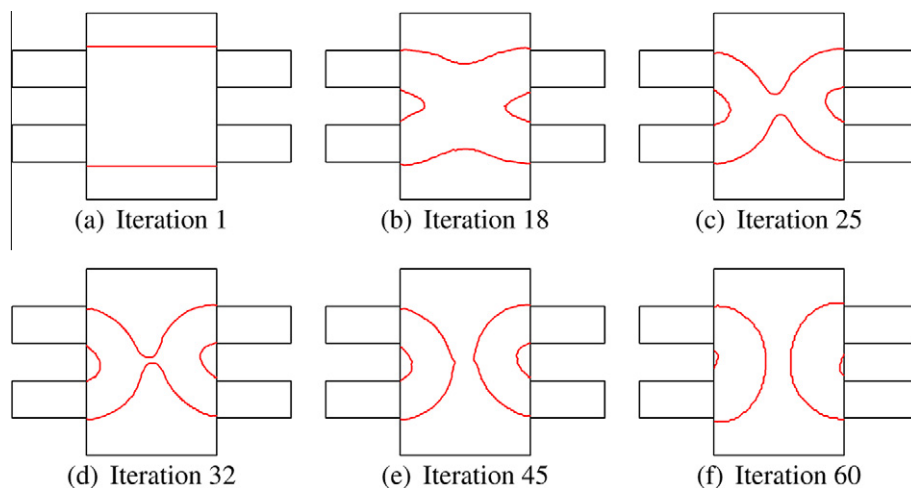


Fig. 7. Snapshots for the evolution and nucleation of the level set in the optimization procedure of the result in Fig. 6(a).

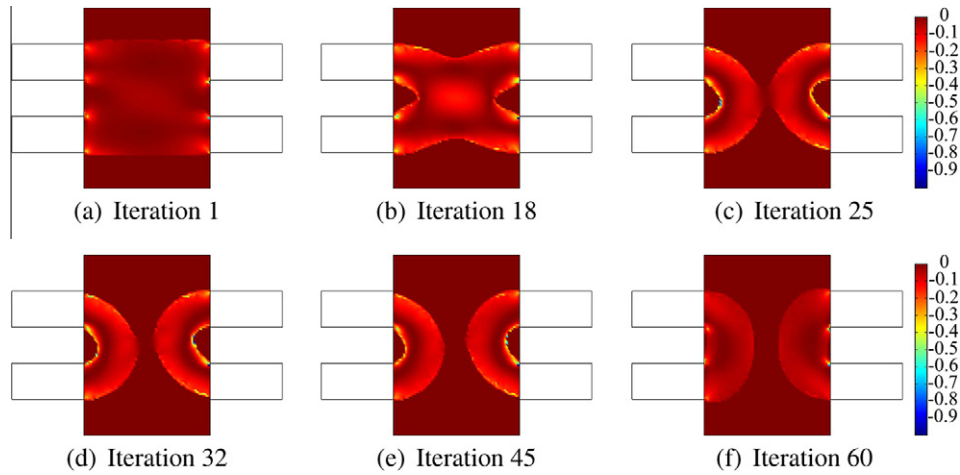


Fig. 8. Snapshots for the shape sensitivity in the optimization procedure of the result in Fig. 6(a).

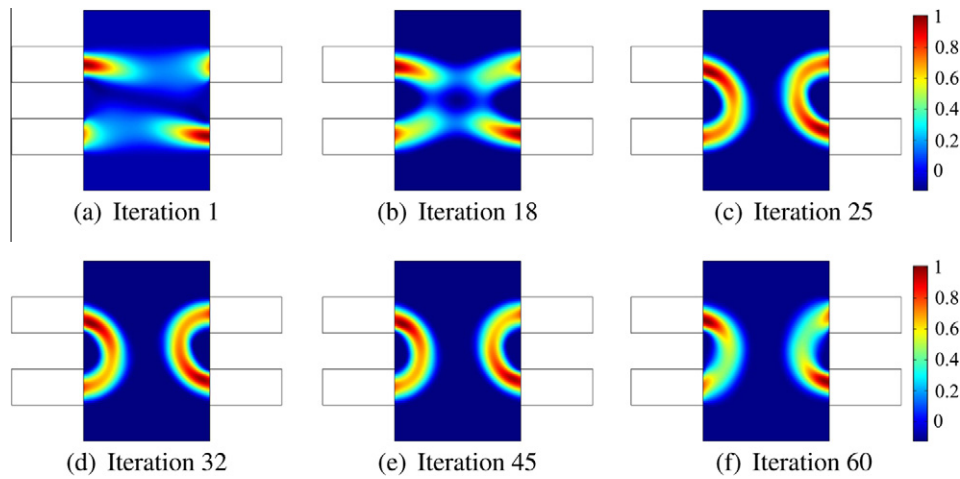


Fig. 9. Snapshots for the topological sensitivity in the optimization procedure of the result in Fig. 6(a).

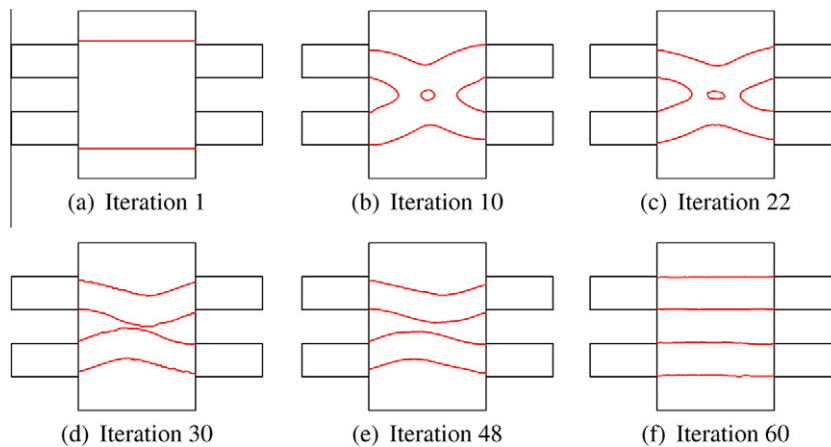


Fig. 10. Snapshots for the evolution and nucleation of the level set in the optimization procedure of the result in Fig. 6(b).

ogy of the four-terminal device and the corresponding distribution of the level set function are shown in Fig. 18(a) and (b). By solving the optimization problem with the same parameter settings for the four-terminal device without body force, the optimal topology is shown in Fig. 18(c). The comparison between the optimized topol-

ogies in Fig. 18(a) and (c) demonstrates that the existence of the gravity results in the change of the topology of the optimized channel. The fluid prone to flow along the direction of the gravity. Therefore, it is really necessary to consider the body force when the design domain has multiple inlets and outlets.

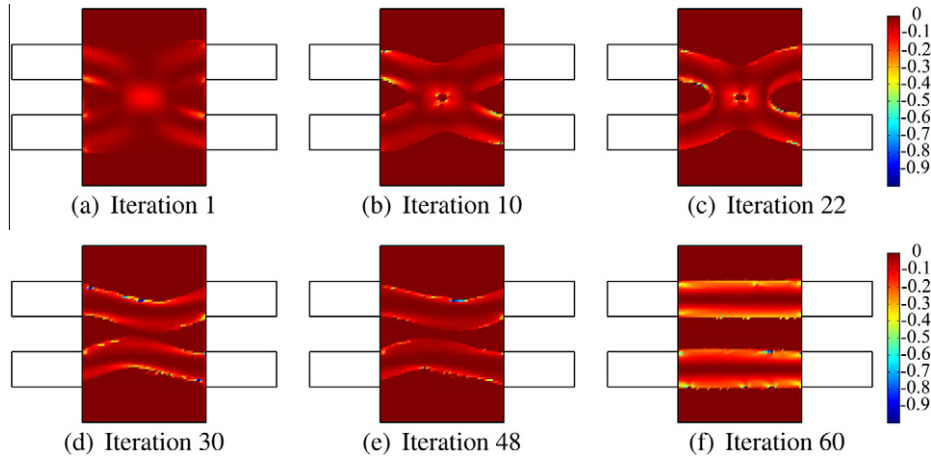


Fig. 11. Snapshots for the shape sensitivity in the optimization procedure of the result in Fig. 6(b).

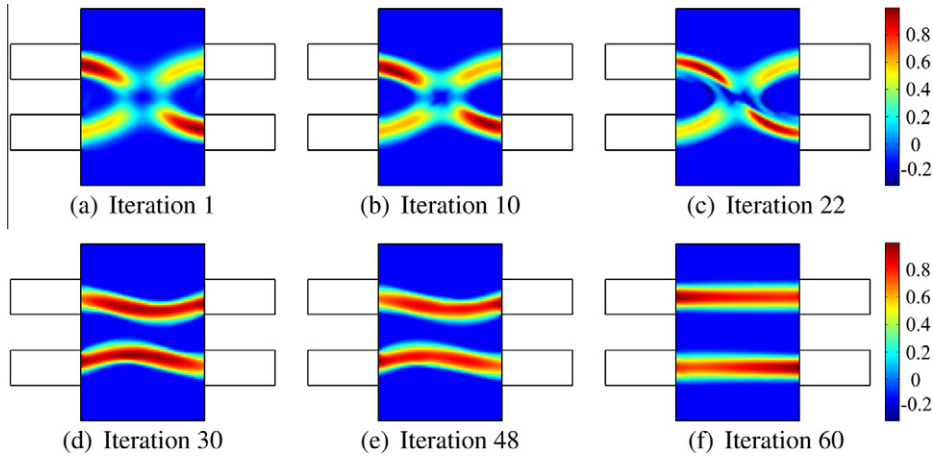


Fig. 12. Snapshots for the topological sensitivity in the optimization procedure of the result in Fig. 6(b).

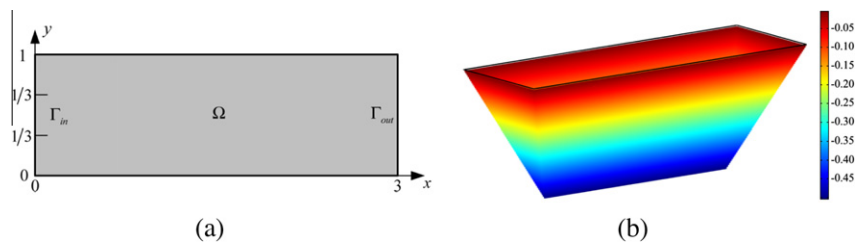


Fig. 13. (a) Optimization domain of the flow in the gravity; (b) initial distribution of the level set function.

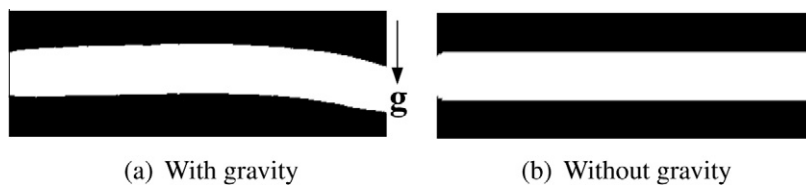


Fig. 14. Optimized topologies of the horizontal channel with or without the gravity.

5.2.3. Siphon in gravity

In the following, a siphon is designed using the topology optimization method. A siphon is a device in which the flow is driven

by the gravity. The optimization domain, used for evolving the level set function, includes two parts Ω_s and Ω_c . Ω_c is the region that is specified as the solid domain ($\mathbf{u} = 0$), and Ω_s is the free

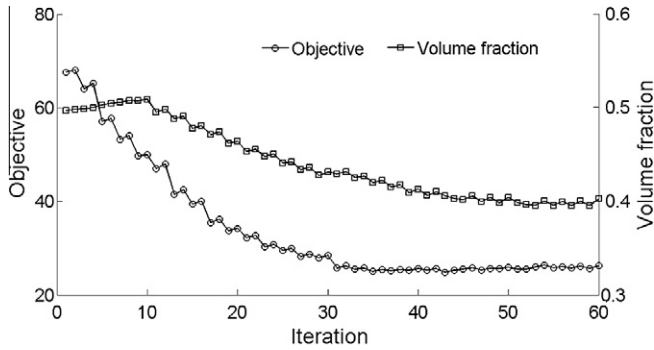


Fig. 15. Convergent histories of the objective value and volume constraint for the optimized flow in the gravity as shown in Fig. 14(a).



Fig. 16. Optimized topology of the horizontal channel for the flow with a given pressure distribution imposed on the inlet of the optimization domain in the gravity.

optimization region during the optimization procedure. The computational domain for the distribution of the fluid velocity and

pressure includes four parts, Ω_d , Ω_s , Ω_c and Ω_r (Fig. 19(a)), where Ω_r is the reservoir and Ω_d is the outlet duct. Based on the above setup, the Hamilton–Jacobi equation (14) can be solved by the finite difference method on the regular rectangular domain. The optimization domain, the reservoir and the outlet duct are discretized by 100×100 , 25×50 , and 50×10 rectangular elements, respectively. The initial level set function is set to be the solution of Eq. (30), where the initial value ϕ_0 is specified as -1 (Fig. 19(b)). By setting the weight of the topological sensitivity ω and the volume fraction of the siphon V^* to be 5 and 0.2 respectively, the optimized siphon (Fig. 20(a)) is obtained by solving the optimization problem in Eq. (12), where the objective is the reverse of the kinetic energy (Eq. (11)). The velocity and level set function distribution in the optimized results are shown in Fig. 20(b) and (c), respectively. Because the inlet of the reservoir is specified to be higher than the outlet duct, a pressure drop is produced by the height difference in the gravity. The pressure drop results in the fluid flowing from the inlet of the reservoir to the outlet duct. This is the siphonal flow occurring in the gravity. Because the solid domain Ω_c is higher than the inlet of the reservoir, the optimized channel balances the effect between the uphill flow and the maximal kinetic energy by tuning the shape and length of the fluid channel. In the siphonal flow, the gravitational potential energy of the fluid is translated into the kinetic energy of the fluid and dissipation of the flow. Therefore, more kinetic energy of the fluid means lower dissipation of the flow. Because the optimization objective is to maximize the kinetic energy, the dissipation power of the flow in the optimized siphon is minimized automatically.

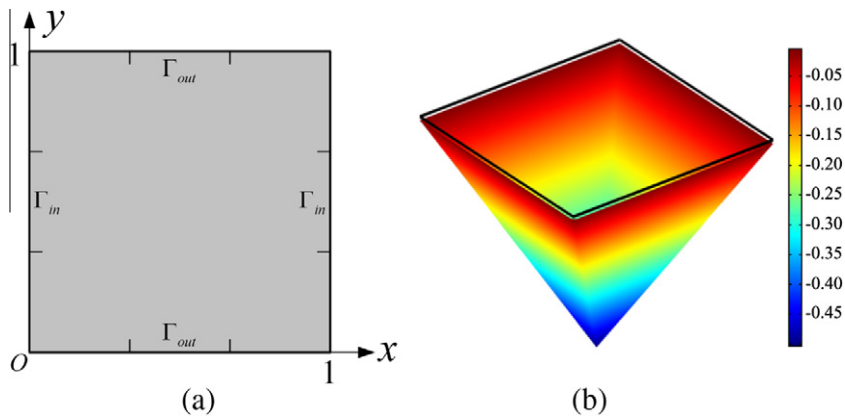


Fig. 17. (a) Optimization domain of the four-terminal device in the gravity; (b) initial distribution of the level set function.

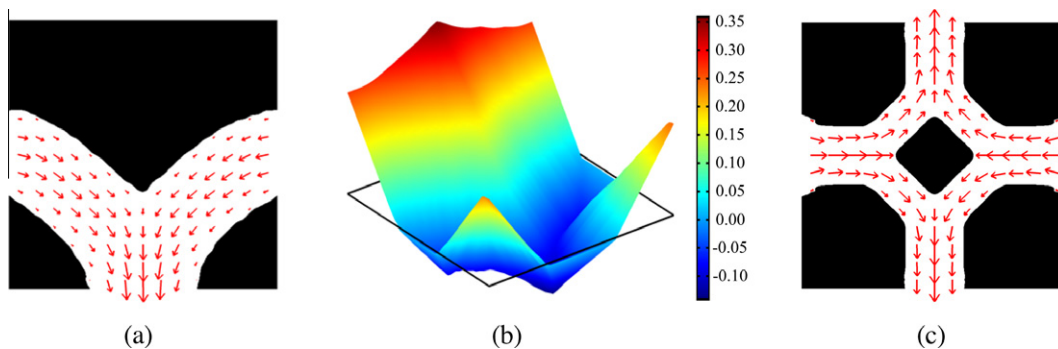


Fig. 18. (a) Optimized topology of the four-terminal device considering the gravity and the corresponding distribution of the fluid velocity vectors; (b) level set function corresponding to the optimized topology; (c) optimized topology of the four-terminal device without the gravity and the corresponding distribution of the fluid velocity vectors.

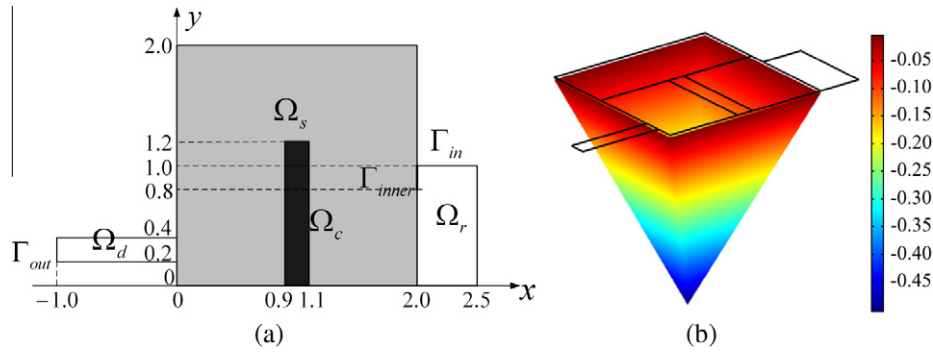


Fig. 19. (a) Optimization domain of the siphon in the gravity. Ω_s is a reservoir to supply the liquid flowing in the siphon; Ω_c is a duct connected to the outlet of the siphon; $\Omega_s \cup \Omega_c$ is the optimization region; the gap Ω_c is a solid region, which is used to ensure the tip of the siphon higher than the inlet of the reservoir Ω_r ; Γ_{in} and Γ_{out} are the inlet and outlet respectively; Γ_{inner} and the left exterior boundaries are set to be no slip type; (b) initial distribution of the level set function defined in $\Omega_s \cup \Omega_c$.

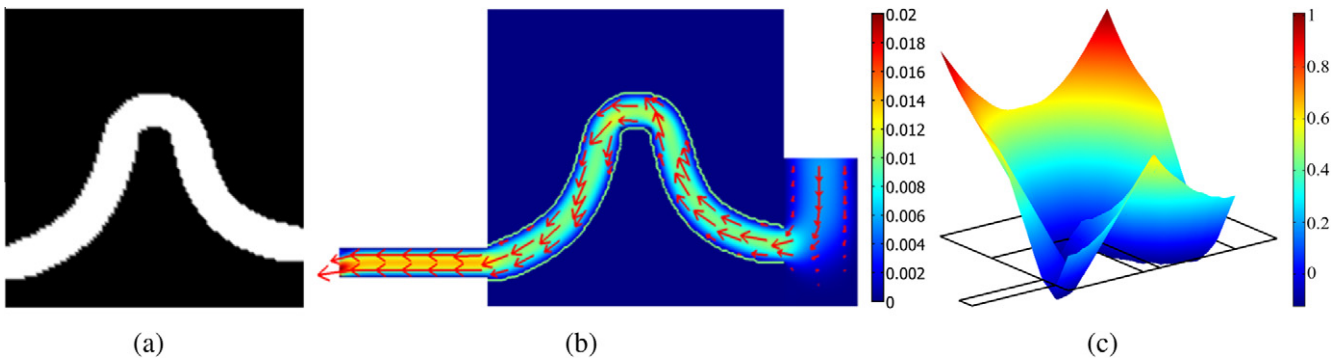


Fig. 20. (a) Optimized topology of the siphon in the gravity; (b) distribution of the fluid velocity; (c) distribution of the level set function.

5.3. Nonuniform and solution-dependent body forces

Optimization of the Navier–Stokes flows with nonuniform and solution-dependent body forces is considered in this section. The nonuniform and solution-dependent body forces are usually used as the driven force in fluid devices, such as the centrifugal chips in microfluidics [53,54]. The nonuniform body force is a function of the spacial coordinate. Because the derivatives of the nonuniform body force with respect to the velocity and pressure are zeros, the nonuniform body force has no appearance in the adjoint equations. The solution-dependent body force depends on the unknowns of physical problems, such as the fluid velocity. Therefore, the adjoint equations have the corresponding terms for the derivatives of the solution-dependent body force with respect to the fluid velocity and pressure as shown in Eq. (17).

5.3.1. Four-terminal device with centrifugal and Coriolis body force

Centrifugal force is a typical body force used to drive fluid flows. In the centrifugal force field, the Coriolis force exists and companies with the centrifugal force. The centrifugal force and the Coriolis force are expressed as $\mathbf{f}_{cen} = (\boldsymbol{\omega} \times \mathbf{r}) \times \boldsymbol{\omega}$ and $\mathbf{f}_{cor} = 2\mathbf{u} \times \boldsymbol{\omega}$ respectively, where $\boldsymbol{\omega}$ is the angular velocity vector and \mathbf{r} is the radial vector of the point inside the flow relative to the rotating center [55]. The centrifugal force and the Coriolis force are nonuniform body force and solution-dependent body force respectively. A four-terminal device in the centrifugal and Coriolis force field is optimized in this numerical example. The optimization domain and the boundary conditions imposed on the inlets and outlets of the four-terminal device are shown in Fig. 17(a). The rotating center is set to be the point with the coordinate (0.5,0.5) which is the center of the optimization domain. The scalar value of the angular speed $\boldsymbol{\omega}$ is set to be 20. The other optimization settings are the

same as that in Section 5.2.2. After solving the optimization problem in Eq. (12), the optimized topologies of the four-terminal device are obtained corresponding to the centrifugal force and the centrifugal–Coriolis force respectively (Figs. 21(a) and 22(a)). The corresponding level set functions are shown in Figs. 21(b) and 22(b). In this numerical example, the rotating center is set to be the center of the optimization domain. Therefore, the centrifugal force distributes symmetrically in the outward direction of the radius vector (Fig. 21(c)). However, because the Coriolis force vector is vertical to the direction of the fluid velocity and along the rotating direction, the distribution of the Coriolis force is not symmetrical (Fig. 22(c)). When only the centrifugal force is considered, the symmetrical optimization domain and symmetrical distribution of the body force determine the symmetrical result in Fig. 21(a) commonly. As the centrifugal force and the Coriolis force are considered simultaneously, the Coriolis force results in the unsymmetrical topology of the four-terminal device in Fig. 22(a).

5.3.2. Double channel with centrifugal and Coriolis body force

A double channel in the centrifugal and Coriolis force field is optimized in the following. Fig. 23(a) is the optimization domain which is discretized by 120×120 rectangular elements. The inlets and outlets of the flow are all set to be open boundaries (Eq. (9)). The initial level set function is set to be the solution of Eq. (30), where the initial value ϕ_0 is specified as -1 (Fig. 23(b)). The rotating center is set to be the point with coordinate of (0.5,2). The scalar value of the angular speed $\boldsymbol{\omega}$ in the clockwise direction is set to be 30. The volume fraction of the fluid is set to be $V^* = 0.3$, and the weight of the topological sensitivity ω is set to be 2. The optimized results for the cases with only centrifugal force and with both the centrifugal force and the Coriolis force are shown in Figs. 24(a) and 25(a) where the optimization objective is the dissipation power in

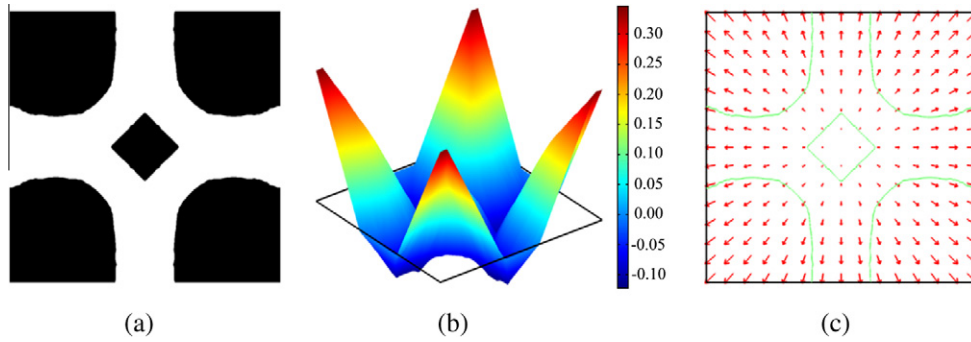


Fig. 21. (a) Optimized topology of the four-terminal device in centrifugal force field; (b) level set function corresponding to the optimized topology; (c) distribution of the centrifugal force.

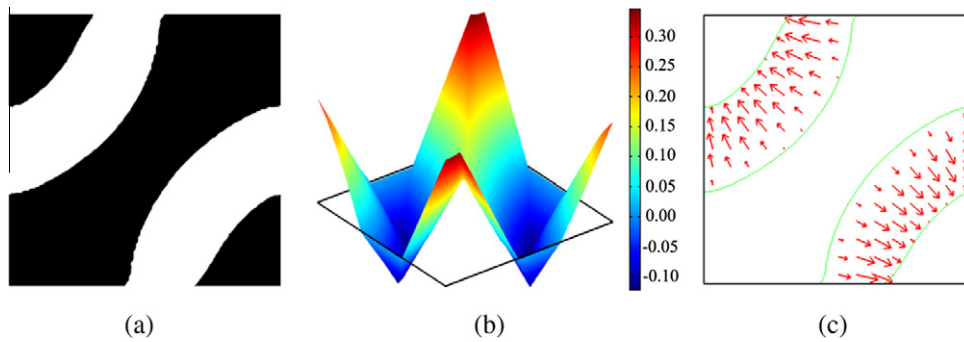


Fig. 22. (a) Optimized topology of the four-terminal device in the centrifugal-Coriolis force field; (b) level set function corresponding to the optimized topology; (c) distribution of the Coriolis force (To manifest the direction of the Coriolis force, the arrows has a different scaling from the centrifugal force).

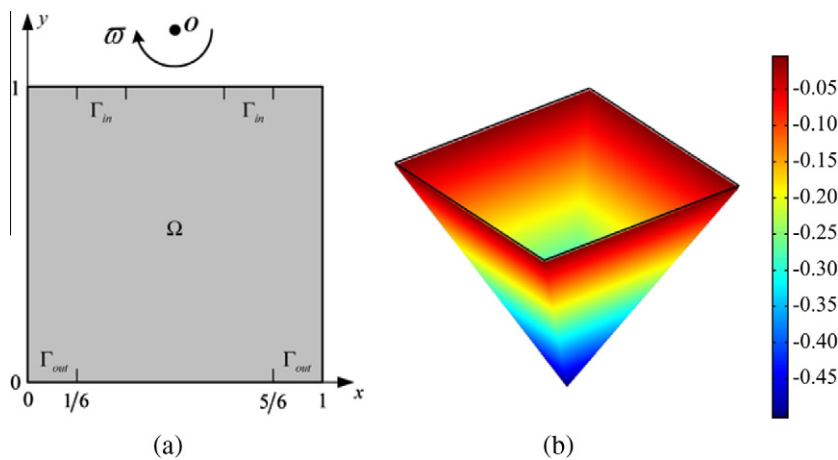


Fig. 23. (a) Optimization domain of the flow in the centrifugal force field; (b) initial distribution of the level set function. The angular speed ω is set to be 30 in the clockwise direction, and the rotating center O is set to be the point with coordinate (0.5,2).

Eq. (10). The convergent histories of the objective value and volume constraint are shown in Fig. 26. Snapshots for the evolving procedure of the level set are shown in Fig. 27. Similar to the numerical example of the four-terminal device in Section 5.3.1, the Coriolis force results in the change of the topology of the optimized fluid channel. Therefore, the Coriolis force deserves to be considered in the design of rotational fluid system.

5.4. Three-dimensional numerical examples

5.4.1. 3D channel with constant body force

For the 3D flow driven by constant body force, the flow in a hexahedron with constant body force is optimized. The optimiza-

tion domain (Fig. 28(a)) is a hexahedron with length, width and height equal to 1, 1 and 0.5, respectively. And it is discretized by $30 \times 30 \times 10$ hexahedral elements. The inlet and outlet of the design domain are set to be open boundaries. The initial level set function is set to be the solution of Eq. (30), where the initial value ϕ_0 is specified as -1 . The constant body force is given as $\mathbf{f} = (10, 10, 0)$. The weight of the topological sensitivity is set to be 3 and the volume fraction of fluid is set to be 0.4. The optimized channel is shown in Fig. 28(b) for the objective of the kinetic energy in Eq. (11). Snapshots for the evolving procedure of the level set are shown in Fig. 29. Fig. 28(b) shows that the optimized channel has a definite lean to the direction of the constant body force, and this results in the work done by the body force. As has been

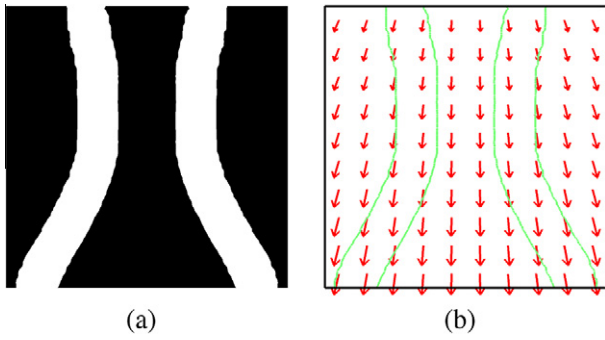


Fig. 24. (a) Optimized topology of the channel in the centrifugal force field; (b) distribution of the centrifugal force vector.

discussed in Section 5.2 for the optimization of the flows in the gravity, the work of the constant body force helps to increase the kinetic energy of the fluid in this example too.

5.4.2. 3D siphon in centrifugal–Coriolis force field

For the 3D flow that is driven by the nonuniform and solution-dependent body forces, a siphon driven by the centrifugal and Coriolis forces is optimized [53,54]. The optimization domain is $\Omega_s \cup \Omega_c$, where Ω_c is a gap filled with solid and enveloped by Ω_s (Fig. 30(a) and (b)). Similar to the 2D siphon example in Section 5.2, Ω_c is specified as a solid region by constraining the fluid velocity to be zero. The optimization domain, the reservoir and the duct are discretized by $100 \times 100 \times 10$, $25 \times 50 \times 6$ and $50 \times 10 \times 6$ hexahedral elements, respectively. The inlet and outlet of the flow are set to be open boundaries. The rotating axis is set to be the axis vertical to the xOy plane at the point $(2.25, 2, 0)$ and the angular velocity is set to be $(0, 0, -100)$. The initial level set function is set to be the solution of Eq. (30), where the initial value ϕ_0 is specified as -1 . By solving the optimization problem with the weight of the topological sensitivity ω and the volume fraction of fluid equal to 20 and 0.2 respectively, the optimized siphon is obtained as shown in Fig. 30(c) and (d) from the different viewpoints, where the objective is the kinetic energy of the flow (Eq. (11)).

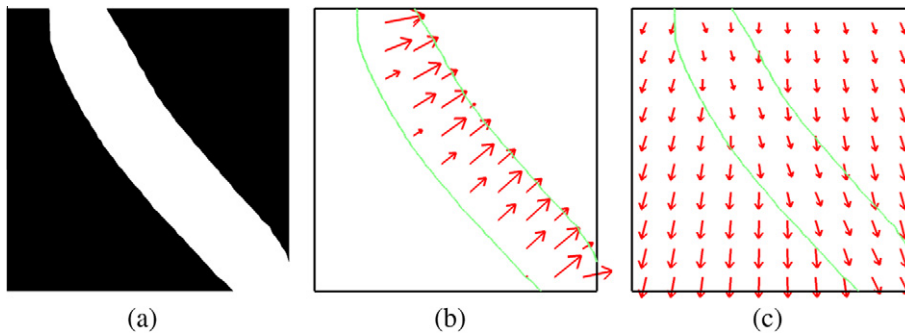


Fig. 25. (a) Optimized topology of the channel in the centrifugal and Coriolis force field; (b) distribution of the Coriolis force vector (To manifest the direction of the Coriolis force, the arrows has a different scaling from the centrifugal force); (c) composition of the centrifugal and Coriolis forces.

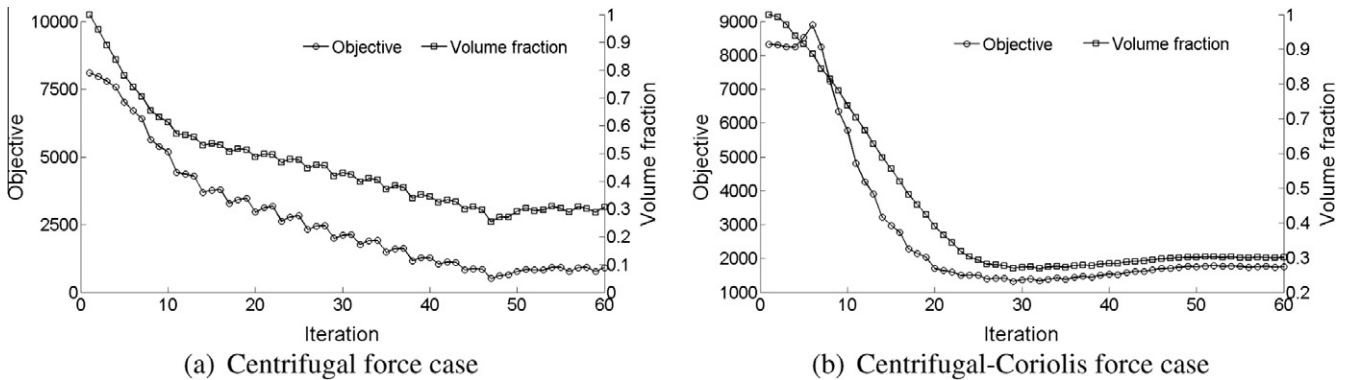


Fig. 26. Convergent histories of the objective value and volume constraint for the topology optimization of the flow with the centrifugal or centrifugal-Coriolis force.

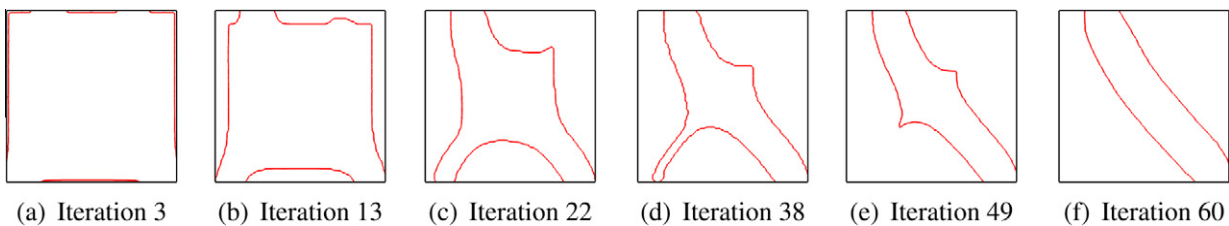


Fig. 27. Snapshots for the evolution and nucleation of the level set in the procedure of the topology optimization of the Navier–Stokes flow with centrifugal-Coriolis force.

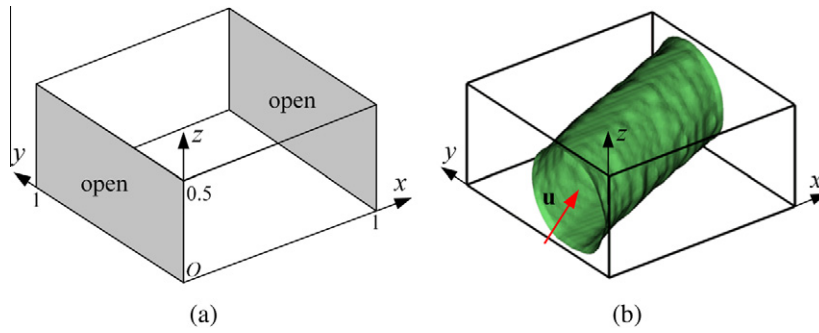


Fig. 28. (a) Optimization domain of the 3D channel in the constant body force field; (b) optimized topology of the channel. The artificial constant body force is set to be $\mathbf{f} = (10, 10, 0)$.

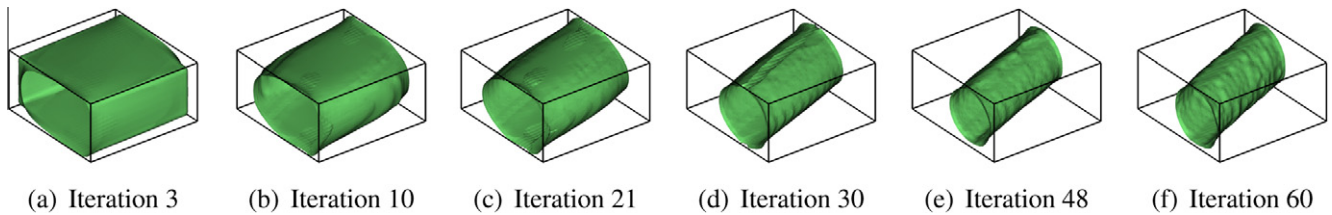


Fig. 29. Snapshots for the evolution and nucleation of the level set in the procedure of the topology optimization of the 3D flow with constant body force.

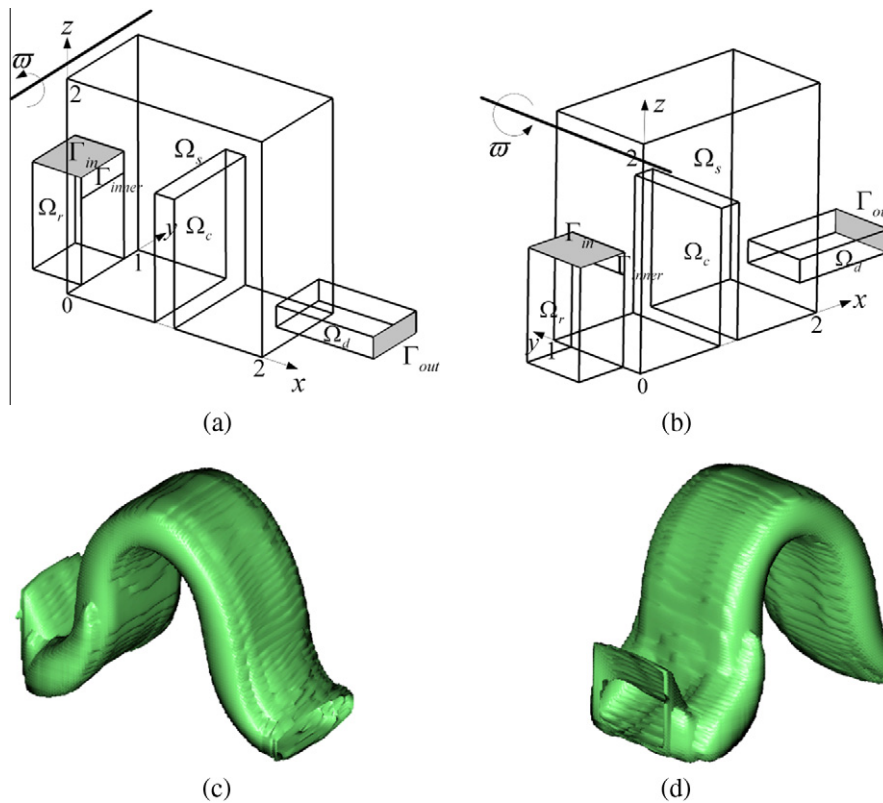


Fig. 30. Optimization domain for the siphon in the centrifugal and Coriolis force field from two different viewpoints (a) and (b). Ω_r is a reservoir to supply the liquid flowing in the siphon; Ω_d is a duct connected to the outlet of the siphon; $\Omega_s \cup \Omega_c$ is the optimization domain; the gap Ω is a solid domain, which is used to ensure the tiptop of the siphon higher than the inlet of the reservoir Ω_r ; Γ_{in} and Γ_{out} are the inlet and outlet respectively; Γ_{inner} and the left exterior boundaries are set to be no slip type. The optimized 3D siphon in the centrifugal and Coriolis body force field is shown in (c) and (d) from two viewpoints corresponding to (a) and (b).

The siphonal flow in the centrifugal force field is similar to that in the gravity. Fig. 30(a) and (b) show that there is a radius difference between the inlet and outlet of the siphon. A pressure drop is pro-

duced by the centrifugal force loaded on the fluid. This pressure drop drives the fluid flowing in the siphon. In the siphonal flow, the potential energy of the fluid is translated into the kinetic en-

ergy and viscous dissipation. Therefore, the optimized siphon tends to increase the kinetic energy and decrease the viscous dissipation in the optimization procedure.

6. Conclusion

Topology optimization method is extended to the Navier–Stokes flows with general body forces by the variational level set method considering the shape and topological sensitivities. The optimization problem is analyzed by the continuous adjoint method. Compared with the discretized adjoint method, the continuous adjoint equations make the optimization procedure more flexible in choosing numerical computational methods that are available to the user. The implicit boundary of the fluid flow is evolved and nucleated by solving the Hamilton–Jacobi equation considering both shape and topological sensitivities. The body forces of the Navier–Stokes flows are considered by categorizing them into constant, nonuniform and solution-dependent types. The numerical examples demonstrated that this method accomplishes the topology optimization of the Navier–Stokes flows with body forces. In this paper, the mainly considered body forces are brought out by the inertia of fluid flow. This topology optimization method is held for the flows of the Newtonian fluid with low and moderate Reynolds numbers. For the high Reynolds number flows or non-Newtonian fluid flows with body forces caused by multiphysical effect, the topology optimization problem needs to be investigated furthermore in the future.

Acknowledgments

This work was supported by the China National High Technology Research and Development Program (863 program) (No. 2012AA040503), the China National Science Fund (Nos. 50975272, 51205381), and SKLAO open fund in CIOMP. The authors are also grateful to the reviewers' kind attention and valuable suggestions.

Appendix A

A.1. Adjoint equations of Navier–Stokes equations with body force

The derivation of the adjoint equations of the Navier–Stokes equations is exhibited in this appendix. According to the Karush–Kuhn–Tucker conditions [48], the variational of \hat{J} in Eq. (16)

$$\delta \hat{J} = \frac{\partial \hat{J}}{\partial \mathbf{u}} \cdot \delta \mathbf{u} + \frac{\partial \hat{J}}{\partial \nabla \mathbf{u}} : \nabla (\delta \mathbf{u}) + \frac{\partial \hat{J}}{\partial p} \delta p + \frac{\partial \hat{J}}{\partial \phi} \delta \phi \quad (31)$$

should be zero corresponding to the optimal distribution of the level set function. This means that the variational of \hat{J} to the velocity \mathbf{u} , the pressure p and the level set function ϕ are all zero

$$\frac{\partial \hat{J}}{\partial \mathbf{u}} \cdot \delta \mathbf{u} + \frac{\partial \hat{J}}{\partial \nabla \mathbf{u}} : \nabla (\delta \mathbf{u}) = 0, \quad \frac{\partial \hat{J}}{\partial p} \delta p = 0, \quad \frac{\partial \hat{J}}{\partial \phi} \delta \phi = 0 \quad (32)$$

Because $\mathbf{u} = \mathbf{0}$ in Ω_c , $(\mathbf{u}, \mathbf{w})_{\Omega_c}$ in Eq. (16) is equal to zero. Based on the first two formulas of Eq. (32), one can obtain

$$J(\delta \mathbf{u}, \nabla \mathbf{u}, p; \phi) + J(\mathbf{u}, \nabla (\delta \mathbf{u}), p; \phi) + a(\delta \mathbf{u}, \mathbf{w})_{\Omega} + b(\delta \mathbf{u}; \mathbf{u}, \mathbf{w})_{\Omega} + b(\mathbf{u}; \delta \mathbf{u}, \mathbf{w})_{\Omega} - \left(\frac{\mathbf{f}}{\partial \mathbf{u}} \cdot \delta \mathbf{u}, \mathbf{w} \right)_{\Omega} - (\nabla \cdot \delta \mathbf{u}, q)_{\Omega} + (H(\phi) \delta \mathbf{u}, \mathbf{w})_{\Omega} = 0$$

$$J(\mathbf{u}, \nabla \mathbf{u}, \delta p; \phi) - (\delta p, \nabla \cdot \mathbf{w})_{\Omega} - \left(\frac{\mathbf{f}}{\partial p} \delta p, \mathbf{w} \right)_{\Omega} = 0 \quad (33)$$

Note that

$$J(\delta \mathbf{u}, \nabla \mathbf{u}, p; \phi) = \int_{\Omega} \left[H(-\phi) \frac{\partial A}{\partial \mathbf{u}} + \tau(\phi) \|\nabla \phi\| \frac{\partial B}{\partial \mathbf{u}} \right] \cdot \delta \mathbf{u} d\Omega = \int_{\Omega} \frac{\partial \tilde{A}}{\partial \mathbf{u}} \cdot \delta \mathbf{u} d\Omega \quad (34)$$

$$J(\mathbf{u}, \nabla \delta \mathbf{u}, p; \phi) = \int_{\Omega} \left[H(-\phi) \frac{\partial A}{\partial \nabla \mathbf{u}} + \tau(\phi) \|\nabla \phi\| \frac{\partial B}{\partial \nabla \mathbf{u}} \right] : \nabla (\delta \mathbf{u}) d\Omega = \int_{\Omega} \frac{\partial \tilde{A}}{\partial \nabla \mathbf{u}} : \nabla (\delta \mathbf{u}) d\Omega = \int_{\Omega} \nabla \cdot \left(\frac{\partial \tilde{A}}{\partial \nabla \mathbf{u}} \cdot \delta \mathbf{u} \right) d\Omega - \int_{\Omega} \left(\nabla \cdot \frac{\partial \tilde{A}}{\partial \nabla \mathbf{u}} \right) \cdot \delta \mathbf{u} d\Omega = \int_{\Gamma_N} \frac{\partial \tilde{A}}{\partial \nabla \mathbf{u}} \cdot \mathbf{n} \cdot \delta \mathbf{u} d\Gamma - \int_{\Omega} \left(\nabla \cdot \frac{\partial \tilde{A}}{\partial \nabla \mathbf{u}} \right) \cdot \delta \mathbf{u} d\Omega \quad (35)$$

$$J(\mathbf{u}, \nabla \mathbf{u}, \delta p; \phi) = \int_{\Omega} \left[H(-\phi) \frac{\partial A}{\partial p} + \tau(\phi) \|\nabla \phi\| \frac{\partial B}{\partial p} \right] \delta p d\Omega = \int_{\Omega} \frac{\partial \tilde{A}}{\partial p} \delta p d\Omega \quad (36)$$

where $\tilde{A} = H(-\phi)A + \tau(\phi) \|\nabla \phi\| B$.

$$a(\delta \mathbf{u}, \mathbf{w})_{\Omega} = -\eta(\Delta \mathbf{w}, \delta \mathbf{u})_{\Omega} + \eta((\nabla \mathbf{w} + \nabla \mathbf{w}^T) \cdot \mathbf{n}, \delta \mathbf{u})_{\Gamma_N} \quad (37)$$

$$b(\delta \mathbf{u}; \mathbf{u}, \mathbf{w})_{\Omega} = (\rho \mathbf{w} \cdot (\nabla \mathbf{u}), \delta \mathbf{u})_{\Omega} \quad (38)$$

$$b(\mathbf{u}; \delta \mathbf{u}, \mathbf{w})_{\Omega} = -(\rho(\mathbf{u} \cdot \nabla) \mathbf{w}, \delta \mathbf{u})_{\Omega} + (\rho(\mathbf{u} \cdot \mathbf{n}) \mathbf{w}, \delta \mathbf{u})_{\Gamma_N} \quad (39)$$

$$(\nabla \cdot \delta \mathbf{u}, q)_{\Omega} = -(\nabla q, \delta \mathbf{u})_{\Omega} + (q \mathbf{n}, \delta \mathbf{u})_{\Gamma_N} \quad (40)$$

where $\Gamma_N = \partial \Omega \setminus \Gamma_D$ is the Neumann boundary. According to the third equation in Eq. 2, one can obtain

$$\begin{cases} \mathbf{u} = \mathbf{0} \Rightarrow \delta \mathbf{u} = \mathbf{0}, & \phi > 0 \\ H(\phi) = 0, & \phi < 0 \end{cases} \quad (41)$$

In addition, the measure of the implicit boundary Γ in Ω is zero. Therefore,

$$(H(\phi) \delta \mathbf{u}, \mathbf{w})_{\Omega} = 0 \quad (42)$$

By combining Eq. (33) with the above equations, one can obtain

$$\int_{\Omega} \left[\frac{\partial \tilde{A}}{\partial \mathbf{u}} - \nabla \cdot \frac{\partial \tilde{A}}{\partial \nabla \mathbf{u}} - \frac{\partial \mathbf{f}}{\partial \mathbf{u}} \cdot \mathbf{w} - \eta \Delta \mathbf{w} + \rho \mathbf{w} \cdot (\nabla \mathbf{u}) - \rho(\mathbf{u} \cdot \nabla) \mathbf{w} + \nabla q \right] \cdot \delta \mathbf{u} d\Omega + \int_{\Gamma_N} \left[\eta(\nabla \mathbf{w} + \nabla \mathbf{w}^T) \cdot \mathbf{n} + \rho(\mathbf{u} \cdot \mathbf{n}) \mathbf{w} - q \mathbf{n} + \frac{\partial \tilde{A}}{\partial \nabla \mathbf{u}} \cdot \mathbf{n} \right] \cdot \delta \mathbf{u} d\Gamma = 0 \quad (43)$$

$$\int_{\Omega} \left[\frac{\partial \tilde{A}}{\partial p} - \frac{\partial \mathbf{f}}{\partial p} \cdot \mathbf{w} - \nabla \cdot \mathbf{w} \right] \delta p d\Omega = 0$$

For the variational of $\mathbf{u} \in \mathcal{H}_E^1(\Omega)$ and $p \in \mathcal{L}^2(\Omega)$ have arbitrariness, the adjoint equations of the Navier–Stokes equations with body force for the topology optimization problem (12) can be obtained as

$$\begin{aligned} -\eta \Delta \mathbf{w} + \rho \mathbf{w} \cdot (\nabla \mathbf{u}) - \rho(\mathbf{u} \cdot \nabla) \mathbf{w} + \nabla q &= -\frac{\partial \tilde{A}}{\partial \mathbf{u}} + \nabla \cdot \frac{\partial \tilde{A}}{\partial \nabla \mathbf{u}} + \frac{\partial \mathbf{f}}{\partial \mathbf{u}} \cdot \mathbf{w} \quad \text{in } \Omega \\ -\nabla \cdot \mathbf{w} &= -\frac{\partial \tilde{A}}{\partial p} + \frac{\partial \mathbf{f}}{\partial p} \cdot \mathbf{w} \quad \text{in } \Omega \end{aligned} \quad (44)$$

$\mathbf{w} = \mathbf{0}$ on Γ_D

$$[-q\mathbf{I} + \eta(\nabla\mathbf{w} + \nabla\mathbf{w}^T)] \cdot \mathbf{n} = -\rho(\mathbf{u} \cdot \mathbf{n})\mathbf{w} - \frac{\partial \tilde{A}}{\partial \nabla \mathbf{u}} \cdot \mathbf{n} \quad \text{on } \Gamma_N$$

A.2. Calculus of shape sensitivity

The shape sensitivity for the topology optimization problem in Eq. (12) can be obtained by the adjoint analysis of the augmented functional in Eq. (16):

$$\begin{aligned} \delta \hat{J} &= \frac{\partial \hat{J}}{\partial \mathbf{u}} \cdot \frac{\partial \mathbf{u}}{\partial \phi} \delta \phi + \frac{\partial \hat{J}}{\partial \nabla \mathbf{u}} : \frac{\partial (\nabla \mathbf{u})}{\partial \phi} \delta \phi + \frac{\partial \hat{J}}{\partial p} \frac{\partial p}{\partial \phi} \delta \phi + \frac{\partial \hat{J}}{\partial \phi} \delta \phi \\ &= \frac{\partial \hat{J}}{\partial \mathbf{u}} \cdot \delta \mathbf{u} + \frac{\partial \hat{J}}{\partial \nabla \mathbf{u}} : \nabla (\delta \mathbf{u}) + \frac{\partial \hat{J}}{\partial p} \delta p + \frac{\partial \hat{J}}{\partial \phi} \delta \phi = \frac{\partial \hat{J}}{\partial \phi} \delta \phi \end{aligned} \quad (45)$$

Based on the first two formulas of Eq. (32), the shape sensitivity can be reduced to

$$\begin{aligned} \delta \hat{J} &= \frac{\partial \hat{J}}{\partial \phi} \delta \phi + \lambda \int_{\Omega} \tau(\phi) \delta \phi \, d\Omega + \int_{\Omega} \tau(\phi) \mathbf{u} \cdot \mathbf{w} \delta \phi \, d\Omega \\ &\quad - \Lambda \int_{\Omega} \tau(\phi) \delta \phi \, d\Omega \left(\int_{\Omega} H(-\phi) \, d\Omega - V^* V_{\Omega} \right) \end{aligned} \quad (46)$$

In addition,

$$\begin{aligned} \delta \|\nabla \phi\| &= \delta \left(\frac{(\nabla \phi)^2}{\|\nabla \phi\|} \right) = \frac{2\nabla \phi \cdot \nabla (\delta \phi)}{\|\nabla \phi\|} - \frac{(\nabla \phi)^2 \cdot \delta \|\nabla \phi\|}{\|\nabla \phi\|^2} \\ &= \frac{2\nabla \phi \cdot \nabla (\delta \phi)}{\|\nabla \phi\|} - \delta \|\nabla \phi\| \end{aligned} \quad (47)$$

Therefore,

$$\delta \|\nabla \phi\| = \frac{\nabla \phi \cdot \nabla (\delta \phi)}{\|\nabla \phi\|} \quad (48)$$

Based on the similar transformation in [27] and Eq. (48), the following transformation can be obtained:

$$\begin{aligned} \frac{\partial \hat{J}}{\partial \phi} \delta \phi &= - \int_{\Omega} \tau(\phi) A \delta \phi \, d\Omega + \int_{\Omega} \delta(\tau(\phi)) \|\nabla \phi\| B \, d\Omega \\ &= - \int_{\Omega} \tau(\phi) A \delta \phi \, d\Omega + \int_{\Omega} [\delta(\tau(\phi)) \|\nabla \phi\| + \tau(\phi) \delta \|\nabla \phi\|] B \, d\Omega \\ &= - \int_{\Omega} \tau(\phi) A \delta \phi \, d\Omega + \int_{\Omega} \left[\delta(\tau(\phi)) \|\nabla \phi\| + \tau(\phi) \frac{\nabla \phi \cdot \nabla (\delta \phi)}{\|\nabla \phi\|} \right] B \, d\Omega \\ &= - \int_{\Omega} \tau(\phi) A \delta \phi \, d\Omega + \int_{\Omega} \left[\delta(\tau(\phi)) \|\nabla \phi\| + \nabla \cdot \left(\tau(\phi) \frac{\nabla \phi}{\|\nabla \phi\|} \delta \phi \right) \right. \\ &\quad \left. - \nabla \cdot \left(\tau(\phi) \frac{\nabla \phi}{\|\nabla \phi\|} \right) \delta \phi \right] B \, d\Omega \\ &= - \int_{\Omega} \tau(\phi) A \delta \phi \, d\Omega + \int_{\Omega} [\delta(\tau(\phi)) \|\nabla \phi\| + \nabla \cdot (\tau(\phi) \mathbf{n}_{\Gamma} \delta \phi) \\ &\quad - \delta \phi \tau(\phi) \nabla \cdot \mathbf{n}_{\Gamma} - \delta(\tau(\phi)) \|\nabla \phi\|] B \, d\Omega \\ &= - \int_{\Omega} \tau(\phi) A \delta \phi \, d\Omega + \int_{\Omega} [\nabla \cdot (\tau(\phi) \mathbf{n}_{\Gamma} \delta \phi) - \delta \phi \tau(\phi) \nabla \cdot \mathbf{n}_{\Gamma}] B \, d\Omega \\ &= - \int_{\Omega} \tau(\phi) A \delta \phi \, d\Omega - \int_{\Omega} \tau(\phi) B \nabla \cdot \mathbf{n}_{\Gamma} \delta \phi \, d\Omega \\ &\quad + \int_{\Omega} [\nabla \cdot (\tau(\phi) \mathbf{n}_{\Gamma} B \delta \phi) - \nabla B \cdot \mathbf{n}_{\Gamma} \tau(\phi) \delta \phi] \, d\Omega \\ &= - \int_{\Omega} \tau(\phi) A \delta \phi \, d\Omega + \int_{\partial \Omega} \tau(\phi) B \delta \phi \mathbf{n}_{\Gamma} \cdot \mathbf{n} \, d\Gamma \\ &\quad - \int_{\Omega} \nabla B \cdot \mathbf{n}_{\Gamma} \tau(\phi) \delta \phi \, d\Omega - \int_{\Omega} \tau(\phi) B \nabla \cdot \mathbf{n}_{\Gamma} \delta \phi \, d\Omega \\ &= - \int_{\Omega} \tau(\phi) A \delta \phi \, d\Omega - \int_{\Omega} \nabla B \cdot \mathbf{n}_{\Gamma} \tau(\phi) \delta \phi \, d\Omega - \int_{\Omega} \tau(\phi) B \kappa \delta \phi \, d\Omega \end{aligned} \quad (49)$$

where $\mathbf{n}_{\Gamma} = \nabla \phi / \|\nabla \phi\|$ and $\kappa = \nabla \cdot \mathbf{n}_{\Gamma}$. Substituting Eq. (49) into Eq. (46), the shape sensitivity for the topology optimization problem in Eq. (12) can be obtained as

$$\begin{aligned} \delta \hat{J} &= - \int_{\Omega} \tau(\phi) A \delta \phi \, d\Omega - \int_{\Omega} \nabla B \cdot \mathbf{n}_{\Gamma} \tau(\phi) \delta \phi \, d\Omega - \int_{\Omega} \tau(\phi) B \kappa \delta \phi \, d\Omega \\ &\quad + \int_{\Omega} \tau(\phi) \mathbf{u} \cdot \mathbf{w} \delta \phi \, d\Omega + \lambda \int_{\Omega} \tau(\phi) \delta \phi \, d\Omega \\ &\quad - \Lambda \left(\int_{\Omega} H(-\phi) \, d\Omega - V^* V_{\Omega} \right) \int_{\Omega} \tau(\phi) \delta \phi \, d\Omega \\ &= - \int_{\Omega} \left[A + \nabla B \cdot \mathbf{n}_{\Gamma} + B \kappa - \mathbf{u} \cdot \mathbf{w} - \lambda + \Lambda \left(\int_{\Omega} H(-\phi) \, d\Omega - V^* V_{\Omega} \right) \right] \\ &\quad \times \tau(\phi) \delta \phi \, d\Omega \end{aligned} \quad (50)$$

References

- [1] M.P. Bendsoe, O. Sigmund, *Topology Optimization Theory Methods and Applications*, Springer, 2003.
- [2] G.P. Steven, Q. Li, Y.M. Xie, Evolutionary topology and shape design for physical field problems, *Comput. Mech.* 26 (2000) 129–139.
- [3] M.P. Bendsoe, N. Kikuchi, Generating optimal topologies in optimal design using a homogenization method, *Comput. Methods Appl. Mech. Engrg.* 71 (1988) 197–224.
- [4] G. Allaire, *Shape Optimization by the Homogenization Method*, Springer-Verlag, New York, 2002.
- [5] G.I.N. Rozvany, Aims scope methods history and unified terminology of computer-aided optimization in structural mechanics, *Struct. Multidisc. Optim.* 21 (2001) 90–108.
- [6] M.P. Bendsoe, O. Sigmund, Material interpolations in topology optimization, *Arch. Appl. Mech.* 69 (1999) 635–654.
- [7] M.Y. Wang, X. Wang, D. Guo, A level set method for structural optimization, *Comput. Methods Appl. Mech. Engrg.* 192 (2003) 227–246.
- [8] G. Allaire, F. Jouve, A. Toader, Structural optimization using sensitivity analysis and a level-set method, *J. Comput. Phys.* 194 (2004) 363–393.
- [9] Z. Liu, J.G. Korvink, Adaptive moving mesh level set method for structure optimization, *Engrg. Optim.* 40 (2008) 529–558.
- [10] X. Xing, P. Wei, M.Y. Wang, A finite element-based level set method for structural optimization, *Int. J. Numer. Methods Engrg.* 82 (2010) 805–842.
- [11] T. Borrvall, J. Petersson, Optimization of fluid in Stokes flow, *Int. J. Numer. Methods Fluids* 41 (2003) 77–107.
- [12] A. Gersborg-Hansen, O. Sigmund, R.B. Haber, Topology optimization of channel flow problems, *Struct. Multidisc. Optim.* 29 (2005) 1–12.
- [13] L.H. Olessen, F. Okkels, H. Bruus, A high-level programming-language implementation of optimization applied to steady-state Navier–Stokes flow, *Int. J. Numer. Methods Engrg.* 65 (2006) 975–1001.
- [14] J.K. Guest, J.H. Prevost, Optimization of creeping fluid flows using a Darcy–Stokes finite element, *Int. J. Numer. Methods Engrg.* 66 (2006) 461–484.
- [15] N. Aage, T.H. Poulsen, A. Gersborg-Hansen, O. Sigmund, Optimization of large scale Stokes flow problems, *Struct. Multidisc. Optim.* 35 (2008) 175–180.
- [16] Y. Deng, Z. Liu, P. Zhang, Y. Wu, J.G. Korvink, Optimization of no-moving-part fluidic resistance microvalves with low Reynolds number, in: *The 23rd IEEE MEMS Conference*, 2010, pp. 67–70.
- [17] B.C. Chen, N. Kikuchi, Topology optimization with design-dependent loads, *Finite Elem. Anal. Des.* 37 (2001) 57–70.
- [18] T. Gao, W.H. Zhang, J.H. Zhu, Topology optimization of heat conduction problem involving design-dependent heat load effect, *Finite Elem. Anal. Des.* 44 (2008) 805–813.
- [19] J.H. Zhu, P. Beckers, W.H. Zhang, On the multi-component layout design with inertial force, *J. Comput. Appl. Math.* 234 (2010) 2222–2230.
- [20] T. Gao, W.H. Zhang, Topology optimization of multiphase material structures under design-dependent pressure loads, *Int. J. Simul. Multidisc. Des. Optim.* 3 (2009) 297–306.
- [21] S. Osher, J.A. Sethian, Front propagating with curvature dependent speed: algorithms based on Hamilton–Jacobi formulations, *J. Comput. Phys.* 78 (1988) 12–49.
- [22] S. Osher, R. Fedkiw, *Level Set Methods and Dynamic Implicit Surfaces*, Springer-Verlag, New York, 2003.
- [23] J.A. Sethian, *Level Set Methods – Evolving Interfaces in Geometry Fluid Mechanics Computer Vision and Materials Science*, Cambridge University Press, 1996.
- [24] R. Malladi, J.A. Sethian, Image-processing via level set curvature flow, *Proc. Natl. Acad. Sci. USA* 92 (2005) 7046–7050.
- [25] M. Sussman, P. Smereka, S. Osher, A level set approach for computing solutions to incompressible 2-phase flow, *J. Comput. Phys.* 114 (1994) 146–159.
- [26] X. Duan, Y. Ma, R. Zhang, Optimal shape control of fluid flow using variational level set method, *Phys. Lett. A* 372 (2008) 1374–1379.
- [27] S. Zhou, Q. Li, A variational level set method for the optimization of steady-state Navier–Stokes flow, *J. Comput. Phys.* 227 (2008) 10178–10195.
- [28] J. Sokolowski, A. Zochowski, On the topological derivative in shape optimization, *SIAM J. Control Optim.* 37 (1999) 1241–1272.

- [29] J. Sokolowski, A. Zochowski, Topological derivatives for elliptic problems, *Inverse Probl.* 15 (1999) 123–134.
- [30] A.A. Novotny, R.A. Feijoo, E. Taroco, C. Padra, Topological sensitivity analysis, *Comput. Methods Appl. Mech. Engrg.* 192 (2003) 803–829.
- [31] M. Burger, B. Hackl, W. Ring, Incorporating topological derivatives into level set methods, *J. Comput. Phys.* 194 (2004) 344–362.
- [32] S. Amstutz, Topological sensitivity analysis for some nonlinear PDE systems, *J. Math. Pure Appl.* 85 (2006) 540–557.
- [33] V.J. Challis, J.K. Guest, Level set topology optimization of fluids in Stokes flow, *Int. J. Numer. Methods Engrg.* 79 (2009) 1284–1308.
- [34] M. Abdelwahed, M. Hassine, Topological optimization method for a geometric control problem in Stokes flow, *Appl. Numer. Math.* 59 (2009) 1823–1838.
- [35] H. Maatoug, Shape optimization for the Stokes equations using topological sensitivity analysis, *ARIMA* 5 (2006) 216–229.
- [36] M.Y. Wang, Shape optimization with level set method incorporating topological derivatives, in: *Sixth Congresses of Struct. Multidisc. Optim.* 2005.
- [37] S. Amstutz, The topological asymptotic for the Navier–Stokes equations, *ESAIM: Control Optim. Calc. Var.* 11 (2005) 401–425.
- [38] S. Zahedi, A.K. Tornberg, Delta function approximations in level set methods by distance function extension, *J. Comput. Phys.* 229 (2010) 2199–2219.
- [39] B. Engquist, A.K. Tornberg, R. Tsai, Discretization of Dirac delta functions in level set methods, *J. Comput. Phys.* 207 (2005) 28–51.
- [40] A.K. Tornberg, B. Engquist, Regularization techniques for numerical approximation of PDEs with singularities, *J. Sci. Comput.* 19 (2003) 1–3.
- [41] V.J. Challis, A discrete level-set topology optimization code written in Matlab, *Struct. Multidisc. Optim.* 41 (2009) 453–464.
- [42] Y. Jung, K.T. Chu, S. Torquato, A variational level set approach for surface area minimization of triply-periodic surfaces, *J. Comput. Phys.* 223 (2007) 711–730.
- [43] P. Michaleris, D.A. Tortorelli, C.A. Vidal, Tangent operators and design sensitivity formulations for transient nonlinear coupled problems with applications to elasto-plasticity, *Int. J. Numer. Methods Engrg.* 37 (1994) 2471–2499.
- [44] J. Nocedal, S.J. Wright, *Numerical Optimization*, Springer, New York, 2000.
- [45] K. Ito, K. Kunisch, *Lagrange Multiplier Approach to Variational Problems and Applications*, SIAM, 2008.
- [46] T. Belytschko, S.P. Xiao, C. Parimi, Topology optimization with implicitly function and regularization, *Int. J. Numer. Methods Engrg.* 57 (2003) 1177–1196.
- [47] T. Slawig, PDE-constrained control using FEMLAB-Control of the Navier–Stokes equations, *Numer. Algorithm* 42 (2006) 107–126.
- [48] M. Hinze, R. Pinnau, M. Ulbrich, S. Ulbrich, *Optimization with PDE Constraints*, Springer, 2009.
- [49] <<http://www.comsol.com>>.
- [50] G. Hauke, T.J.R. Hughes, A unified approach to compressible and incompressible flows, *Comput. Methods Appl. Mech. Engrg.* 113 (1994) 389–395.
- [51] S. Osher, R. Fedkiw, *Level Set Methods and Dynamic Implicit Surfaces*, Springer-Verlag, New York, 2003.
- [52] C. Min, On reinitializing level set functions, *J. Comput. Phys.* 229 (2010) 2764–2772.
- [53] J. Ducrée, S. Haeblerle, S. Lutz, S. Pausch, F. Stetten, R. Zengerle, Design and fabrication of a centrifugally driven microfluidic disk for fully integrated metabolic assays on whole blood, *J. Microeng. Microeng.* 17 (2007) 103–115.
- [54] J. Steigert, T. Brenner, M. Grumann, L. Riegger, R. Zengerle, J. Ducrée, Design and fabrication of a centrifugally driven microfluidic disk for fully integrated metabolic assays on whole blood, in: *IEEE MEMS Conference*, vol. 229, 2006, pp. 2764–2772.
- [55] <<http://scienceworld.wolfram.com/physics/Navier-StokesEquationsRotational.html>>.